Wind and Wave Climate in the Arctic Ocean as Observed by Altimeters

QINGXIANG LIU

Physical Oceanography Laboratory/Qingdao Collaborative Innovation Center of Marine Science and Technology, Ocean University of China, Qingdao, China, and Faculty of Science, Engineering and Technology, Swinburne University of Technology, Melbourne, Victoria, Australia

ALEXANDER V. BABANIN

Department of Infrastructure Engineering, University of Melbourne, and Faculty of Science, Engineering and Technology, Swinburne University of Technology, Melbourne, Victoria, Australia

STEFAN ZIEGER

Bureau of Meteorology, Melbourne, Victoria, Australia

IAN R. YOUNG

Department of Infrastructure Engineering, University of Melbourne, Melbourne, Victoria, Australia

CHANGLONG GUAN

Physical Oceanography Laboratory/Qingdao Collaborative Innovation Center of Marine Science and Technology, Ocean University of China, Qingdao, China

(Manuscript received 14 March 2016, in final form 27 July 2016)

ABSTRACT

Twenty years (1996–2015) of satellite observations were used to study the climatology and trends of oceanic winds and waves in the Arctic Ocean in the summer season (August–September). The Atlantic-side seas, exposed to the open ocean, host more energetic waves than those on the Pacific side. Trend analysis shows a clear spatial (regional) and temporal (interannual) variability in wave height and wind speed. Waves in the Chukchi Sea, Beaufort Sea (near the northern Alaska), and Laptev Sea have been increasing at a rate of 0.1–0.3 m decade^{-1}, found to be statistically significant at the 90% level. The trend of waves in the Greenland and Barents Seas, on the contrary, is weak and not statistically significant. In the Barents and Kara Seas, winds and waves initially increased between 1996 and 2006 and later decreased. Large-scale atmospheric circulations such as the Arctic Oscillation and Arctic dipole anomaly have a clear impact on the variation of winds and waves in the Atlantic sector. Comparison between altimeter observations and ERA-Interim shows that the reanalysis winds are on average 1.6 m s^{-1} lower in the Arctic Ocean, which translates to a low bias of significant wave height (-0.27 m) in the reanalysis wave data.

1. Introduction

The Arctic sea ice, as an early signal of global climate change (e.g., Walsh 1991), has continuously declined over the modern satellite era. The downward trend of the Arctic sea ice extent is deemed to have been accelerated significantly since the last decade as a result of the complicated feedback mechanisms between thermodynamic and dynamic processes in the Arctic (Stroeve et al. 2012; Serreze and Stroeve 2015). Not only is the ice cover retreating rapidly, but the ice thickness is also severely reduced, featuring a gradual transition from perennial multiyear ice to first-year ice (Maslanik et al. 2007). In the meantime, earlier onset of summer melt together with a delay of autumn reformation is also reported, leading up to an intensified shortening of ice persistence (Frey et al. 2015). Since 2007, a series of extreme September ice extent minima have been

Corresponding author address: Alexander V. Babanin, University of Melbourne, Parkville VIC 3010, Australia.
E-mail: a.babanin@unimelb.edu.au

DOI: 10.1175/JCLI-D-16-0219.1

reported, and the lowest ever recorded minimum of $3.39 \times 10^6\,km^2$, occurring in 2012, only amounted to 54% of the 1981–2010 average minimum.

The impact of such extensive loss of the Arctic ice on the atmospheric and oceanic systems is very significant. In the context of ocean surface waves, the most intuitive influence is that it enlarges the open-water area and consequently increases the effective fetch (e.g., Thomson and Rogers 2014). Combined with favoring atmospheric conditions, energetic wave events may be expected to emerge more frequently in the Arctic marginal ice zones (MIZs). When propagating through sea ice and ice floes, waves experience a series of scatter and dissipation events by the heterogeneous ice terrain, and as a result high-frequency components of wave spectra can be totally reflected or dissipated in MIZs (Squire et al. 1995, 2009). However, as demonstrated in Collins et al. (2015), energetic swells have the potential to break up an ice shield with thickness of 0.5–0.6 m in a rather short time through mechanical strain and then propagate uninhibitedly. This wave-induced open area in MIZs allows additional wave growth and more solar heating of the upper ocean because of the so-called ice-albedo feedback (Perovich et al. 2007), which in turn accelerates the ice melt. Although this positive ice–wave feedback has not been quantified yet, it would exacerbate ice retreating and to some extent intensify the advent of a seasonally ice-free Arctic (Wang and Overland 2012; Thomson and Rogers 2014). The simulated rate of the Arctic sea ice retreat by the current climate models is generally slower than the observed one (Jeffries et al. 2013), indicating parameterizations of important processes such as wave–ice interaction should be included. Furthermore, as a link between the atmospheric boundary layer and the upper ocean mixed layer, the emerging ocean waves also play a crucial role in the momentum, energy, mass, heat, and gas exchange across the air–sea interface. We refer the reader to Babanin (2011, ch. 9) and Cavaleri et al. (2012) for a detailed discussion on this topic. Other wave-related impacts in the Arctic include the acceleration in coastal erosion rate due to the enhanced wave action on thawing and vulnerable shorelines (Overeem et al. 2011; Jeffries et al. 2013) and the safety threats to the increasing offshore activities and Arctic shipping (Smith and Stephenson 2013). All these issues provide strong motivation to characterize the wave climate in the Arctic Ocean over the past several decades.

Studies on the Arctic ice extent/area climate have been continuously reported in the literature (e.g., Parkinson et al. 1999; Comiso and Nishio 2008). In contrast, the wave climate in the Arctic Ocean has been less investigated and only waves in a few subregions of the Arctic Ocean have been studied, based on altimeter observations (Francis et al. 2011) and wave hindcasts and/or reanalyses (Semedo et al. 2015; Wang et al. 2015; Thomson et al. 2016). All of these data sources have their strengths and weaknesses (e.g., Gulev and Grigorieva 2006; Zieger 2010). Compared to the reanalyses, altimeter observations are relatively sparse but provide a homogeneous and accurate description of the sea state in the past approximately three decades, while the limitation of the reanalyses is that their performance strongly depends on the state-of-the-art models and the quality of external forcing such as bathymetry, wind fields, and sea ice cover. The wave–ice interaction is not clearly understood and is oversimplified in the present third-generation (3G) wave models (e.g., Tolman 2003; Dobrynin et al. 2014; Rogers and Zieger 2014). Hence, wave height simulated by wave models in the Arctic MIZs should be interpreted with caution. Zieger et al. (2013) and Babanin et al. (2014) initially studied the wave climate in the Arctic Ocean as observed by satellite altimeters. Here we present a more detailed and comprehensive analysis of the wave climate and its trends in the entire Arctic basin-scale over the past two decades (1996–2015). Recently Stopa et al. (2016b) also carried out a study on the wave climate in the Arctic on the basis of a wave hindcast and altimeter measurements, focusing on the seasonality and trends of the sea state. Since winds are the driving force of ocean surface waves, we also included the wind climate in the Arctic Ocean as observed by satellite altimetry. Altimeters estimate wind speed from backscatter, which is related to the mean square slope of the sea surface (Chelton et al. 2001).

This paper is organized as follows. Section 2 details all the data used in this study and the relevant analysis methods. Section 3 presents our main results for wind and wave climate and their trends in the Arctic Ocean, as well as analyses of their interannual and regional variability. To assess the regional variability of wind and wave climate, we adopted the regional masks developed by Parkinson et al. (1999) and Meier et al. (2007), which divided the Arctic Ocean into selected subregions: the Beaufort Sea, Chukchi Sea, East Siberian Sea, Laptev Sea, Kara Sea, Barents Sea, Greenland Sea, and Baffin Bay (Fig. 1). The discussion in section 4 compares our measurements with one widely used reanalysis dataset, and explains its possible limitations. Impacts of the large-scale atmospheric circulations, including the Arctic Oscillation and Arctic dipole anomaly, on changes of winds and waves are also investigated in this section with an attempt to explain the abrupt decrease in extreme

TABLE 1. Altimeter data and calibration used in this study. The asterisk refers to the calibrated value of wave height H_s and wind speed U_{10}. Wind speed was derived from the Abdalla (2012) wind model, a transfer function of radar backscatter $f(\sigma_0)$, with specific offset σ_0^{offset} applied to minimize the RMSE between altimeter estimated U_{10} and in situ buoy measurements [see Zieger et al. (2009) for methodology].

Altimeter	Year (Aug + Sep)	H_s calibration	σ_0^{offset}	U_{10} calibration
ERS-2	1996–99	$H_s^* = 1.076 \times H_s + 0.042$	+0.075 dB	$U_{10}^* = 1.043 \times f(\sigma_0 + \sigma_0^{\text{offset}}) - 0.071$
—	2000	—	—	$U_{10}^* = 0.980 \times f(\sigma_0 + \sigma_0^{\text{offset}}) - 0.119$
—	2001–02	—	—	$U_{10}^* = 0.972 \times f(\sigma_0 + \sigma_0^{\text{offset}}) - 0.036$
Envisat	2002–11	$H_s^* = 0.981 \times H_s + 0.132$	−0.086 dB	$U_{10}^* = 1.026 \times f(\sigma_0 + \sigma_0^{\text{offset}}) - 0.232$
CryoSat-2	2010–15	$H_s^* = 0.949 \times H_s - 0.004$	−0.008 dB	$U_{10}^* = 1.050 \times f(\sigma_0 + \sigma_0^{\text{offset}}) - 0.369$

wave height and wind speed in the Barents Sea in the summer of 2011. Section 5 summarizes the main conclusions of the paper.

2. Data and methods

a. Altimeter database

Radar altimeters onboard satellites are capable of providing high-quality ocean surface wave (H_s) measurements and reasonable wind (U_{10}) observations. Because of their good global coverage and long duration, these observations have been extensively used in the literature, including studies on wave and wind climate (e.g., Young et al. 2011), calibration and validation of numerical wave models (e.g., Ardhuin et al. 2010; Stopa et al. 2016a; Zieger et al. 2015), and intercomparison of meteorological reanalyses (e.g., Caires et al. 2004; Stopa and Cheung 2014). For the detailed techniques of satellite altimetry, the reader is referred to Chelton et al. (2001). In general, the noisy returned radar signals from the rough ocean surface are averaged into 1-Hz records for practical applications, which normally characterize the oceanographic parameters over footprints ranging from 1 to 10 km. For a specific satellite mission, the real extent of its global coverage is defined by its orbital parameters. In this regard, the coverage of altimeters operated by NASA and the Centre National d'Études Spatiales (CNES; i.e., TOPEX and *Jason-1/2*) resolves less than 66°N/S, while altimeters launched by the European Space Agency cover up to ~82° [i.e., *European Remote-Sensing Satellites 1* and *2* (*ERS-1/2*) and *Envisat*] or even higher (88° for *CryoSat-2*). Measurements from three missions, namely *ERS-2*,[1] *Envisat*, and *CryoSat-2* over the past two decades (1996–2015) are used in our study to investigate wave and wind climate in the Arctic Ocean (Table 1). Because of the seasonal variability of the Arctic ice extent, waves present in this specific region experience a dramatic change in fetch toward the end of summer (Thomson and Rogers 2014). Only two boreal summer months (August and September) are taken into account in this study, during which the maximum open-ocean area and thus wave fetch are expected (e.g., Comiso and Nishio 2008; Wang et al. 2015). We further merged the altimeter observations of these two calendar months and regarded the finally obtained results as a proxy for the whole summer season.

Altimeter measurements are not free of errors and data "spikes" (outliers) among them should be carefully discerned and eliminated before further research. The fully calibrated and validated multiplatform altimeter database described in Zieger et al. (2009) is extended for this study. The original 1-Hz measurements from each altimeter mission are first checked by a three-pass quality-control process and then calibrated and validated by quasi-simultaneous measurements from in situ buoys and other altimeter platforms. Table 1 summarizes the calibrations of H_s and U_{10} we adopted for each mission. The processed wave height (H_s) and wind speed (U_{10}) generally have a root-mean-square error (RMSE) within 0.2 m and 1.3 m s^{-1}, respectively [see Table 4 of Zieger et al. (2009)]. Although the calibration and validation of altimeter measurements (H_s and U_{10}) were mostly undertaken in low and middle latitudes, observations in high-latitude zones are expected to be of the same quality level. As demonstrated in Francis et al. (2011), *Envisat*-estimated wave heights exhibit a very strong correlation (0.96) with their offshore in situ measurements in the southeastern Chukchi Sea. To further validate our altimeter data, we compared them against records from four buoys (red circles in Fig. 1) in the Chukchi Sea. These in situ data were sourced from the National Data Buoy Center (NDBC; http://www.ndbc.noaa.gov) and are only available in summer seasons since 2012. Applications of these high-latitude stations can also be seen in Bernier et al. (2016), Francis et al. (2016, manuscript submitted to *J. Geophys.*

[1] In June 2003, *ERS-2*'s onboard tape recorder experienced a number of failures and consequently limited its coverage in the North Atlantic. Therefore we only used *ERS-2* data before 2003.

FIG. 1. Subregions of the Arctic Ocean used for regional analysis as defined by Parkinson et al. (1999) and Meier et al. (2007) and the four NDBC buoys (red open circles) used for validation of altimeter H_s and U_{10} measurements.

Res.), and Stopa et al. (2016b). Figure 2 presents the collocated altimeter-buoy data, for which only collocations within 50-km radius and 1-h temporal separation were considered. A total of 56 (134) sample points were obtained for H_s (U_{10}) measurements, yielding a correlation coefficient of 0.95 (0.93) and an RMSE of 0.25 m (1.15 m s^{-1}), which prove that the performance of altimeter data in the Arctic is as good as what we have seen in other geographical basins.

b. *Sea ice classification*

Figure 3 presents *Envisat* observations in the Arctic Ocean for (top) March and (bottom) September 2007, including (left) the mean H_s and (right) the number of valid 1-Hz altimeter samples for each 1° × 1° bin. Data were filtered by the standard ice flag within altimeter data records and the three-pass quality control procedure detailed in Zieger et al. (2009). In September 2007 (Fig. 3, bottom), the Beaufort Sea, the western Laptev Sea, and the Fram Strait were covered by sea ice (see Fig. 4, bottom, for the distribution of sea ice extent in this month), resulting in the very few sample points by altimeter in these regions. Inspection of March 2007 (Fig. 3, top), however, shows that considerable wave observations were available in the northern part of the Chukchi and Laptev Seas. This is an unexpected behavior because apart from the North Atlantic sector, the Arctic Ocean should be covered by ice in March as this is the end of winter and features the maximum sea ice extent of that same year (e.g., Comiso and Nishio 2008; Maslanik et al. 2011). As in Babanin et al. (2014), we attribute these ''unrealistic'' waves to errors of measurements, interpretation, or

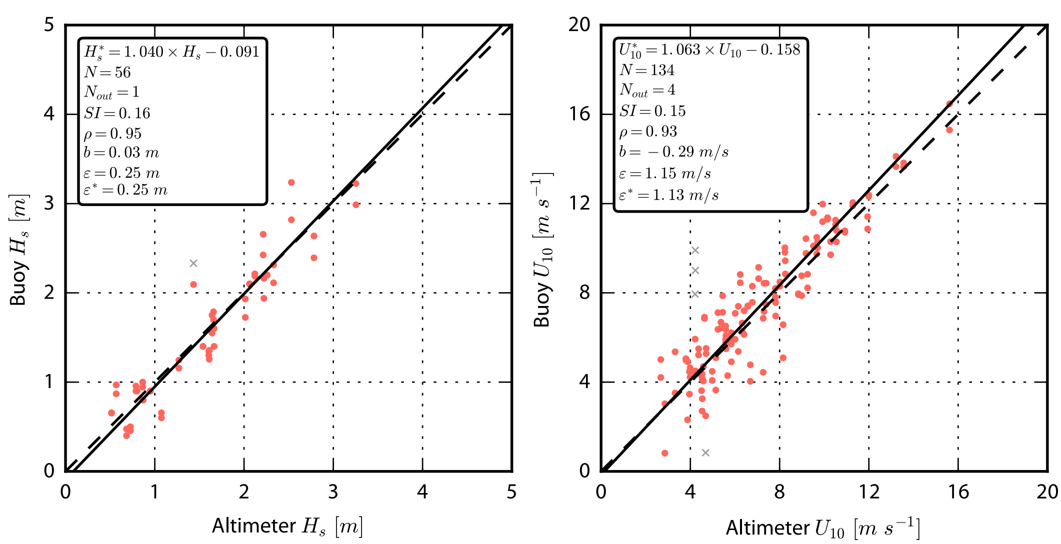

FIG. 2. Comparison between altimeter measurements and buoy observations: (left) wave height H_s and (right) wind speed U_{10}. Collocated measurements are considered within 50-km radius and 1-h temporal separation. The solid line represents the reduced-major-axis (RMA) fit and the dashed line is the 1:1 line. Error statistics for scatter index (SI), correlation coefficient ρ, bias b, RMSE ε, and number N of sample points are given in the inset, with outliers N_{out} (detected by robust regression) labeled with gray crosses. The term ε* signifies the RMSE after the RMA correction. For the technical details, please refer to Zieger et al. (2009) and Liu et al. (2016).

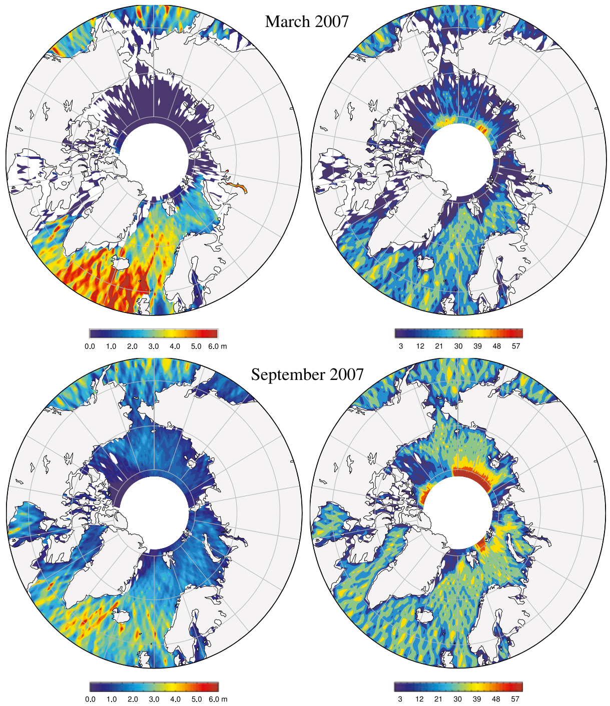

FIG. 3. *Envisat* observations in the Arctic Ocean binned to 1° × 1° for (top) March and (bottom) September 2007. Color shades show (left) mean significant wave height (m) and (right) the corresponding number of records that make up the average. The standard ice flags within the altimeter data records and the three-pass quality control procedure in Zieger et al. (2009) were used to eliminate invalid records.

data processing. Another likely cause is the spatiotemporal variability of ice cover. Altimeters might occasionally encounter open water within their footprints (e.g., leads and polynyas) and report the instantaneous wave heights, which are necessarily low because of the very limited fetches. In any case, these spurious waves, if not excluded, would bias our final statistics and climatology. This also suggests that the standard ice flag is not accurate enough and necessitates a reliable algorithm to identify sea ice occurrence. The selected algorithm should be versatile and applicable to various missions.

Envisat was equipped with various remote sensing instruments, including a dual-frequency radar altimeter and a dual-channel microwave radiometer. Tran et al. (2009) developed a well-tested three-parameter (i.e., the Ku-band radar backscatter, the difference and average of the dual-channel brightness temperatures) classifier to map sea ice from altimeter measurements. Instruments such as the dual-channel radiometer are, however, not available on all altimeter platforms. Hence, we adopted a universal algorithm that depends on altimeter backscatter only. Because of the heterogeneous nature of sea ice (e.g., leads, cracks, and ripples), individual altimeter waveforms exhibit a greater variability than those from the open water. Following Laxon (1990) and Rinne and Skourup (2012) a threshold value for the standard deviation of Ku-band backscatter was used to detect waveforms over sea ice. For the threshold a value of 0.2 dB was found to provide optimal results in comparison to the three-parameter classifier proposed by Tran et al. (2009). The validation of the one-parameter classifier against the three-parameter one was performed for the entire *Envisat* data (cycles 6–113). Individual *Envisat* data records (1 Hz) that were identified as sea ice were counted and compared. These two mapping algorithms showed, on average, a 92.4% agreement. Figure 4 shows the comparison of sea ice maps for two *Envisat* cycles 25 (March 2004; Fig. 4, top) and 61 (September 2007; Fig. 4, bottom). The one-parameter classifier (Fig. 4, right) is in both instances able to reproduce the sea ice extent obtained from the three-parameter mapping algorithm (Fig. 4, left). The marginal differences between the two algorithms mainly appear in MIZs, suggesting that wave statistics in the MIZs obtained with the one-parameter approach should also be interpreted with caution. The threshold value of 0.2 dB for the standard deviation of Ku-band radar backscatter was applied to all altimeter missions used in this study.

c. *Averaging area*

Because of the nadir-pointing geometry and the narrow swath of satellite altimetry, the 1-Hz altimeter records should be resampled into larger bins for climate research (e.g., Young 1994; Hemer et al. 2010; Young et al. 2011). In the global basin, the widely used bin size is 1° × 1° and 2° × 2° (e.g., Vinoth and Young 2011). The number of altimeter transects traversing each bin depends on the size and the latitude of the bin in question. Zieger et al. (2014) analyzed ground-track patterns of various altimeters and found that a 2° × 2° bin contains samples from 10 to 14 day month^{-1} in midlatitudes in 1995, when two altimeters were operated simultaneously. A higher sampling rate is expected at high latitudes due to the orbit configuration. In the Arctic, an equal-spaced Cartesian grid is a better choice than a uniform spherical grid because the meridians converge at the North Pole. We thus remapped altimeter data onto a Cartesian grid using a north polar stereographic projection. Two different bin sizes (i.e., 75 × 75 km^2 and 200 × 200 km^2, hereinafter G75 and G200) are illustrated in Fig. 5, showing the mean H_s and sampling rate provided by *Envisat* from August to September 2007. Using larger bin size moderates the mean sea state and enlarges the sampling frequency (Figs. 5c,d vs Figs. 5a,b),

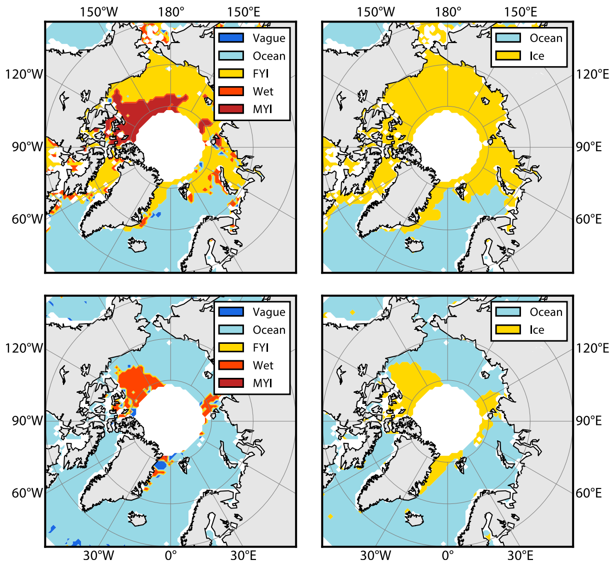

FIG. 4. Sea ice maps for (top) *Envisat* cycle 25 (8 Mar–12 Apr 2004) and (bottom) cycle 61 (20 Aug–24 Sep 2007) based on (left) the three-parameter classifier (Tran et al. 2009) and (right) the one-parameter classifier. Color codes for (left) dark blue is vague, light blue is open water, yellow is first-year ice, orange is wet ice, and brown is multiyear ice. In (right), light blue indicates open water and yellow is ice. Altimeter data were binned into a 75 km × 75 km grid.

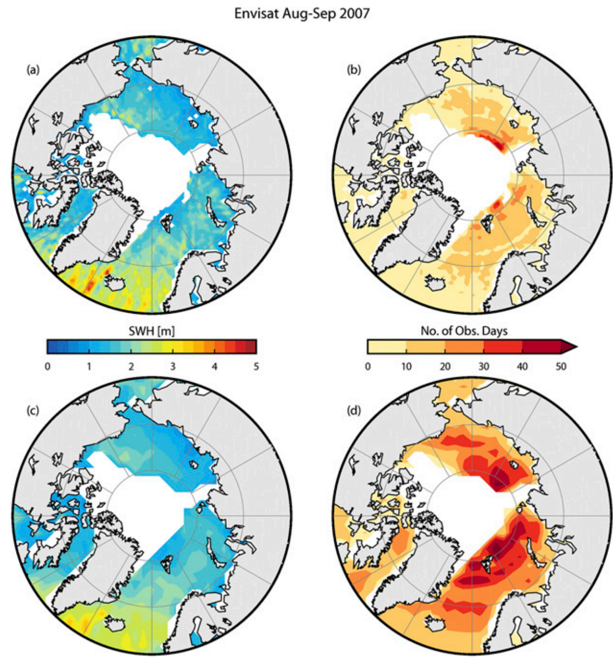

FIG. 5. (a),(c) The mean wave height and (b),(d) the sampling days given by the *Envisat* altimeter in the Arctic area from August through September 2007 for different cell sizes: (top) 75 × 75 km^2 and (bottom) 200 × 200 km^2.

leading to a more smooth and realistic wave field. The streaklike patterns present in the G75 bins (Fig. 5a; see also Fig. 3), as a signature of altimeter ground tracks, become negligible in the G200 bins (Fig. 5c). Each G75 bin contains observations from 10 to 20 days in the two summer months (Fig. 5b), while 20–40 observing days or higher can be founded in the G200 bins (Fig. 5d). The latter is comparable to the sampling rate reported by Zieger et al. (2014), which is capable of reproducing buoy-estimated climatological mean values. Based on these results, we selected a bin size of 200 × 200 km^2 for further analysis. It is worth noting that the adoption of a larger bin size would result in unrealistic statistics in the proximity of coastlines and small islands. As shown in Figs. 5c and 5d, the G200 bins spread across Novaya Zemlya archipelago in between the Kara Sea and the Barents Sea, the Canadian Arctic Archipelago around Baffin Bay, and so forth. In view of the unreliability of the coastal performance of altimeters, the sea states around these poorly resolved islands are not of practical interest here.

d. Trend estimation

All valid altimeter records from 1996 to 2015 were binned to 200 × 200 km^2 bins and mean as well as 90th and 99th percentiles were computed from the data. The "Type M" method described in Tuomi et al. (2011) is applied to calculate all the statistics from the ice-free altimeter records. It should be remembered that because of the limitation of the altimeter sampling patterns, the 90th and 99th percentile U_{10} and H_s values estimated by altimeters might be biased low compared to buoy measurements. To test for significance of the trend the Mann–Kendall test (MKT) was selected. The MKT is a nonparametric test of randomness against trend (Mann 1945; Kendall 1955) and is robust against outliers and missing values. It is particularly well suited for assessing the trend in short/noisy time series (e.g., our 20-yr statistics). It has been extensively applied in hydrology (e.g., Hirsch et al. 1982), and in the context of oceanic wind and wave climate it was used in a number of studies (e.g., Wang and Swail 2001; Young et al. 2011; Zieger et al. 2014; Stopa and Cheung 2014). Frey et al. (2015) applied the MKT to identify trend in sea ice persistence in the Bering, Chukchi, and Beaufort Seas. The Sen estimator (Sen 1968) is used to calculate the magnitude of trend from yearly statistics. Autocorrelation in time can influence the level of significance in the test and bias the test statistic of the MKT. To exclude the effect of autocorrelation in time the variance of the Mann–Kendall statistic was corrected based on the method presented in Hamed and Rao (1998). Each trend was tested for statistical significance at the 90% level.

e. Additional data

The sea ice age data (Tschudi et al. 2015) archived at U.S. National Snow and Ice Data Center (NSIDC; http://nsidc.org/) was used to show the change of ice extent in summer (August and September) over the past two decades. Both the temporal resolution and spatial resolution of this dataset are higher compared to the binned altimeter data. The sea ice archive contains weekly estimates of sea ice type (including first-year ice and multiyear ice) for the Arctic Ocean and is based on remotely sensed data of sea ice motion and sea ice extent. The data are stored on a 12.5-km Northern Hemisphere Equal-Area Scalable Earth Grid (Brodzik et al. 2012) and are available for the period from November 1978 to December 2012. Maslanik et al. (2007, 2011) contains a detailed description of this dataset.

Two reanalysis datasets, namely ERA-Interim (Dee et al. 2011) and the NCEP–NCAR reanalysis (Kalnay et al. 1996) were used to compare and confirm our results (see section 4). The Arctic Oscillation index from the U.S. National Centers for Environmental Information (NCEI) and the Arctic dipole index from Overland et al. (2012) were used to study correlations between large-scale atmospheric modes and the variability of oceanic winds and waves.

3. Results

a. Climate over the past two decades

1) Wind speed

The climatology by means of average and 90th and 99th percentiles of summer wind speed and wave height in the Arctic Ocean over the past two decades is presented in Fig. 6. The overall average wind speed across the Arctic is approximately $8\,\mathrm{m\,s^{-1}}$ (Fig. 6a). Winds over the East Siberian Sea and Baffin Bay are about $7.0\,\mathrm{m\,s^{-1}}$. The southeast area of the Chukchi Sea, the Beaufort Sea, and the Laptev Sea show a slightly stronger wind ($8\,\mathrm{m\,s^{-1}}$) with the highest winds located in the Greenland and Norwegian Seas, particularly in the vicinity of Iceland ($9.5\,\mathrm{m\,s^{-1}}$), which is related to the Icelandic low off the southeast coast of Greenland (Serreze and Barry 2014) and the extratropical storm track in the North Atlantic. The Barents and Kara Seas characterize an average U_{10} around $7.5\,\mathrm{m\,s^{-1}}$. The climatology of altimeter wind speed (Fig. 6a) is in good agreement with those derived from reanalysis datasets. Wang et al. (2015) showed that the maximum values of average U_{10} of the Beaufort–Chukchi–Bering Seas appear in the north and west Alaskan coast (their Fig. 2c), and Semedo et al. (2015) reported that the south of Iceland features the maximum of average U_{10} in the Nordic seas (including the Greenland, Norwegian, and Barents Seas; see their Fig. 1b).

The spatial distribution of the 90th percentile of wind speed (Fig. 6b) shares the similar pattern with the mean values. One exception is that the 90th percentile winds are largest between Greenland and Iceland ($15\,\mathrm{m\,s^{-1}}$) rather than to the south of Iceland. According to Hughes and Cassano (2015), this change is due to the strong barrier jets that developed in the Denmark Strait. The polar easterlies directed toward the high and steep Greenland plateau are unable to ascend the topography and as a result are forced to turn left into a strong, near-surface jet along the southeast of coast of Greenland (Harden et al. 2011; Harden and Renfrew 2012). Winds (90th percentile) over other subregions are roughly comparable at $12\,\mathrm{m\,s^{-1}}$ with the only exception of the East Siberian Sea, showing a minimum less than $9\,\mathrm{m\,s^{-1}}$. Note that such relatively low values might be the result of a low sample size (years) in these regions. The thick black line north of the East Siberian Sea in Fig. 6b indicates a region that was covered by sea ice for more than 10 years and therefore the wind speed estimated by altimeter possibly biased compared to the real climatological value. The 99th percentile of wind speed (Fig. 6c) exhibits more spatial variability than the two statistical metrics discussed before. Now the Atlantic-side seas (including the Barents and Kara Seas) characterize an apparent higher extreme wind ($>16\,\mathrm{m\,s^{-1}}$) than those Pacific-side seas ($\sim13\,\mathrm{m\,s^{-1}}$). This is consistent with the fact that cyclonic weather systems are more frequent on the Atlantic side of the Arctic Ocean (Serreze and Barry 2014, see their Fig. 4.9). Storms generated along the North Atlantic storm track frequently penetrate into the Barents and Kara Seas from the south and southwest. On the Pacific side, the semipermanent low pressure center of action, namely the Aleutian low, disappears as a mean feature in summer and relatively few cyclones can migrate into the Arctic Ocean (Serreze and Barry 2014). In addition, the strongest U_{10} located in Denmark Strait ($\sim18\,\mathrm{m\,s^{-1}}$) corresponds well with the two regions of enhanced barrier wind activity shown in Harden et al. (2011).

2) Wave height

The climatology of significant wave height shows a similar but slightly smoother spatial pattern compared to that of wind speed. For the mean value (Fig. 6d), the smallest waves ($\sim$1.1 m) were found in the southernmost East Siberian Sea. The Chukchi, Beaufort, Laptev, and Kara Seas are dominated by about 1.5-m waves. Consistent with wind speed, the maximum wave height (2.8 m) appears around the southeast coast of Greenland and south of Iceland, followed by the 2.2-m waves in

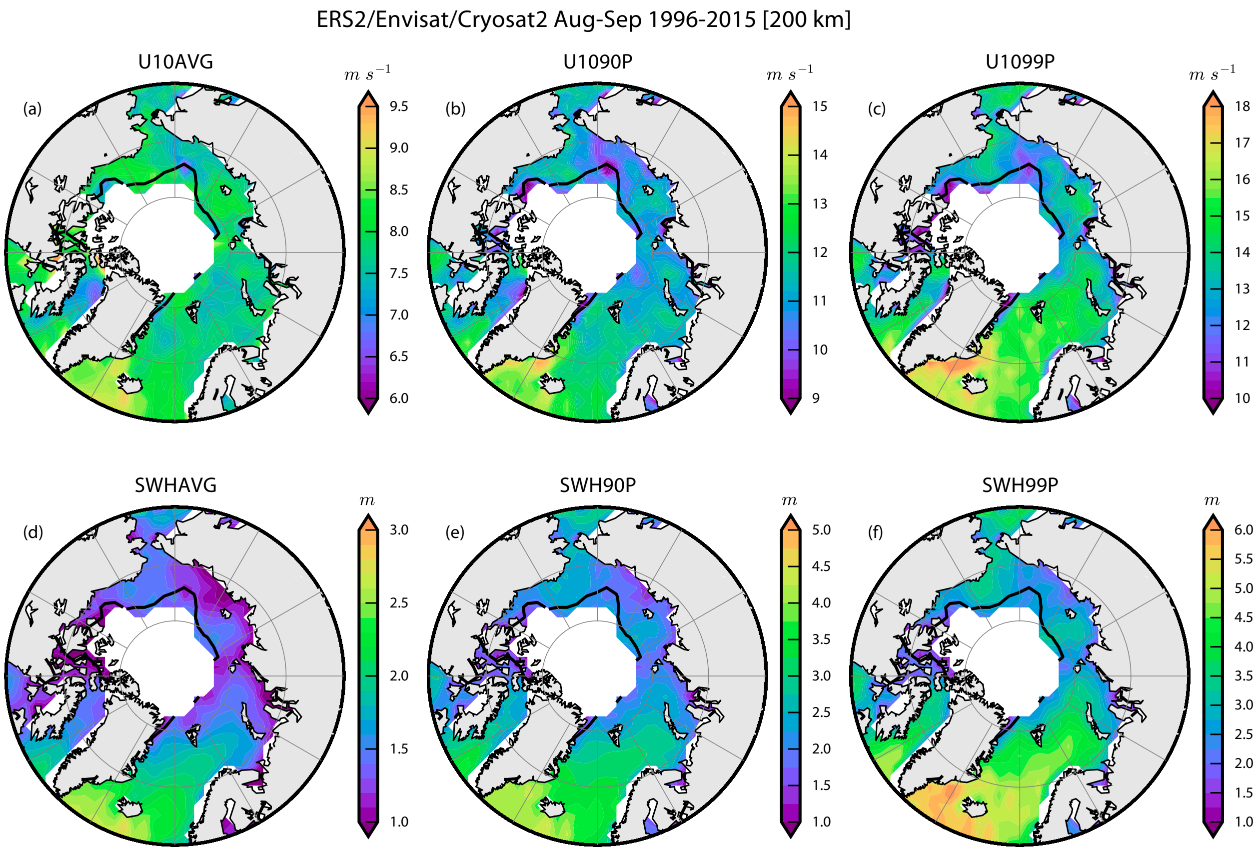

FIG. 6. The climatology of (top) wind speed and (bottom) wave height in the Arctic Ocean as observed by altimeter over summer months (August and September) from 1996 through 2015, for the (a),(d) average and (b),(e) 90th and (c),(f) 99th percentiles, respectively. The thick black line shows the contour line of 10 sampling years by altimeter.

the Norwegian and eastern Greenland Seas and then 1.8 m waves present in the Barents Sea. Again, these patterns are in line with those from reanalysis data [see Fig. 4c of Wang et al. (2015), Fig. 2b of Semedo et al. (2015), and Fig. 10d herein]. Waves in the Chukchi and Beaufort Seas appear to be dominated by wind sea [the mean wave period is generally less than 5 s; see Fig. 6 of Wang et al. (2015)], while the majority of the Norwegian and Barents Seas is dominated by westerly and southwesterly long period swell in the summer seasons [see Fig. 4 of Semedo et al. (2015)]. As a result, the wave patterns on the Pacific side generally follow the wind patterns but this is not strictly the case for the Atlantic sector, particularly in the Barents and Kara Seas, where the intrusion of northeastward swell is clearly reproduced by our altimeter data. A recent model study by Stopa et al. (2016b) also supports this argument, showing that in summer the wind sea wave height H_{sw} is 2–3 times the swell wave height H_{ss} in the Pacific-side seas, and H_{ss} is ~1 m higher than H_{sw} in the Atlantic sector.

The 90th percentile wave height (Fig. 6e) shows the similar patterns as the mean values (Fig. 6d). The maximum value of 4.5-m wave height was found south of Iceland while the minimum value of 2.0-m wave height was located in the East Siberian Sea. Figure 6f shows the 99th percentile of wave height. The most energetic waves appear in the proximity of Iceland and the maximum 99th percentile H_s (>6 m) emerges in the Denmark Strait as a response of the strong barrier jets in this region. The 99th percentile H_s is approximately 5 m in the Norwegian and Barents Seas. The southeastern Chukchi Sea, the Laptev Sea, and the Kara Sea generally show wave heights of about 3–4 m and the East Siberian Sea is the most modest (<3 m). Another energetic region is the southern part of the Baffin Bay, where the extreme waves are 5 m in height due to the extreme wind speed (16 m s^{-1}; Fig. 6c). One detail that should be made clear is that the relatively high 99th percentile of H_s (Fig. 6f) in the Barents and Kara Seas is related to the relatively high extreme wind speed (Fig. 6c), which is a result of the penetration of storms from the North Atlantic track. The intrusion of swell into these regions as explained for the mean H_s is not relevant here. A good illustration of this rationality can be seen in Semedo et al. (2015, their Figs. 2 and 3). They demonstrated that although to a good degree the Norwegian Sea is dominated by swell in the winter months, the extreme waves (represented by 99th percentiles) are in fact mostly generated by the local winds.

b. Trend over the past two decades

1) WIND SPEED

The trend (Sen's slope; section 2d) of summer wind speed and wave height in the Arctic Ocean over the past two decades is presented in Fig. 7. Markers (plus signs) indicate whether the trend was statistically significant at 90% level. In general, the trend of mean oceanic U_{10} (Fig. 7a) is dominated by a negative trend. Winds over the Greenland Sea (between Svalbard and Iceland) decreased at a rate of $\sim -0.4\,\mathrm{m\,s^{-1}\,decade^{-1}}$. A slightly stronger downward trend ($\sim -0.6\,\mathrm{m\,s^{-1}\,decade^{-1}}$) was found in the East Siberian and Laptev Seas. The regions west and north of the Alaskan coast, around the Novaya Zemlya archipelago, and in the southern Baffin Bay show an upward trend about 0.3–$0.5\,\mathrm{m\,s^{-1}\,decade^{-1}}$. According to Fig. 6a, the mean U_{10} in the eastern Greenland Sea is $\sim 8\,\mathrm{m\,s^{-1}}$, so an absolute trend of $-0.4\,\mathrm{m\,s^{-1}\,decade^{-1}}$ in this region is equivalent to a relative trend of $-0.5\%\,\mathrm{yr^{-1}}$, agreeing well with the values reported by Stopa et al. (2016b). There are, however, inconsistencies between the trends computed from our altimeter data and those from reanalyses, particularly in the Chukchi, East Siberian, and Laptev Seas. In the East Siberian Sea, Wang et al. (2015, their Figs. 7a,c) and Stopa et al. (2016b) reported positive trends in U_{10}, contrary to what we found here. These inconsistencies possibly result from the different sampling seasons, data sources, and durations considered in these studies. It should be remembered that altimeters can only provide wind speed when their footprints are ice free but both Wang et al. (2015) and Stopa et al. (2016b) analyzed the entire wind data, including the winds over ice covers.

Trends in the 90th and 99th percentile winds speed (Figs. 7b,c) share similar patterns and are generally positive except those in the Greenland Sea. In 1996–2015, the Fram Strait and the Denmark Strait are the two regions having the highest downward trends ($\sim 1\,\mathrm{m\,s^{-1}\,decade^{-1}}$) in the extreme wind speed (99th percentile; Fig. 7c). Outside the Greenland Sea, the 99th percentile U_{10} values basically have increased at a rate greater than $0.5\,\mathrm{m\,s^{-1}\,decade^{-1}}$ with the maximum values ($2\,\mathrm{m\,s^{-1}\,decade^{-1}}$) present in the central Chukchi Sea, the northern Laptev Sea, and the seas around the Novaya Zemlya archipelago.

2) WAVE HEIGHT

Unlike the wind speed, the mean and 90th and 99th percentiles of wave height basically have changed in a consistent way over the past two decades (1996–2015; Figs. 7d–f). For the mean H_s (Fig. 7d), the regions with statistically significant upward trends include the Chukchi, Laptev, and Kara Seas and Baffin Bay. Waves in these regions have increased at a rate greater than $0.1\,\mathrm{m\,decade^{-1}}$. The maximum positive trends of wave height (0.3–$0.4\,\mathrm{m\,decade^{-1}}$) appeared in the Laptev Sea, followed by trends of $\sim 0.3\,\mathrm{m\,decade^{-1}}$ north of the Alaskan coast. The overall trends of H_s in the Greenland–Norwegian–Barents Seas are weak and not statistically significant, except that waves around the coast of Iceland have increased somewhat (0.05–$0.1\,\mathrm{m\,decade^{-1}}$). The trends of mean H_s presented here also agree well with previous studies. The pioneering work of Francis et al. (2011) showed upward trends of $0.02\,\mathrm{m\,yr^{-1}}$ in the southeast Chukchi Sea and 0.03–$0.04\,\mathrm{m\,yr^{-1}}$ near the northern Alaskan coast in 1993–2010 (see their Figs. 3 and 4), which are basically the same as our results (Fig. 7d). This is not surprising because both Francis et al. (2011) and our work are based on the analysis of the altimeter-sensed wave height. Using the reanalysis dataset for the period 1971–2013, Wang et al. (2015) reported a 0.02–$0.03\,\mathrm{m\,yr^{-1}}$ increasing rate of waves near the north of coast of Alaska, consistent with the altimeter-based studies (their Fig. 7; see also Stopa et al. 2016b). In the west of Alaskan coast, our increasing rates of $0.2\,\mathrm{m\,decade^{-1}}$ coincides with the positive trend of U_{10} we found in Fig. 7a, while this is not clear in the reanalyses (e.g., Wang et al. 2015). In the Greenland–Norwegian–Barents Seas, Semedo et al. (2015) reached the same conclusion as ours from their high-resolution reanalysis data that the linear trends of summer waves are close to zero and are not statistically significant.

The distributions of the trends of the 90th and 99th percentiles H_s (Figs. 7e,f) are similar to that for mean H_s. It is worth mentioning that both 99th percentile H_s (Fig. 7f) and U_{10} (Fig. 7c) values have decreased slightly in the Denmark Strait, implying there might be a decrease in the intensity of barrier jets in summer of 1996–2015.

c. Interannual and regional variability

Since 2007, the Arctic sea ice extent has reached a series of extreme minima. All the nine lowest September ice extents have all occurred within the past nine years (e.g., Serreze and Stroeve 2015; see also Fig. 9 herein). Significant atmospheric circulation anomalies have been articulated in a number of studies (e.g., Wang et al. 2009; Overland et al. 2012; Ogi and

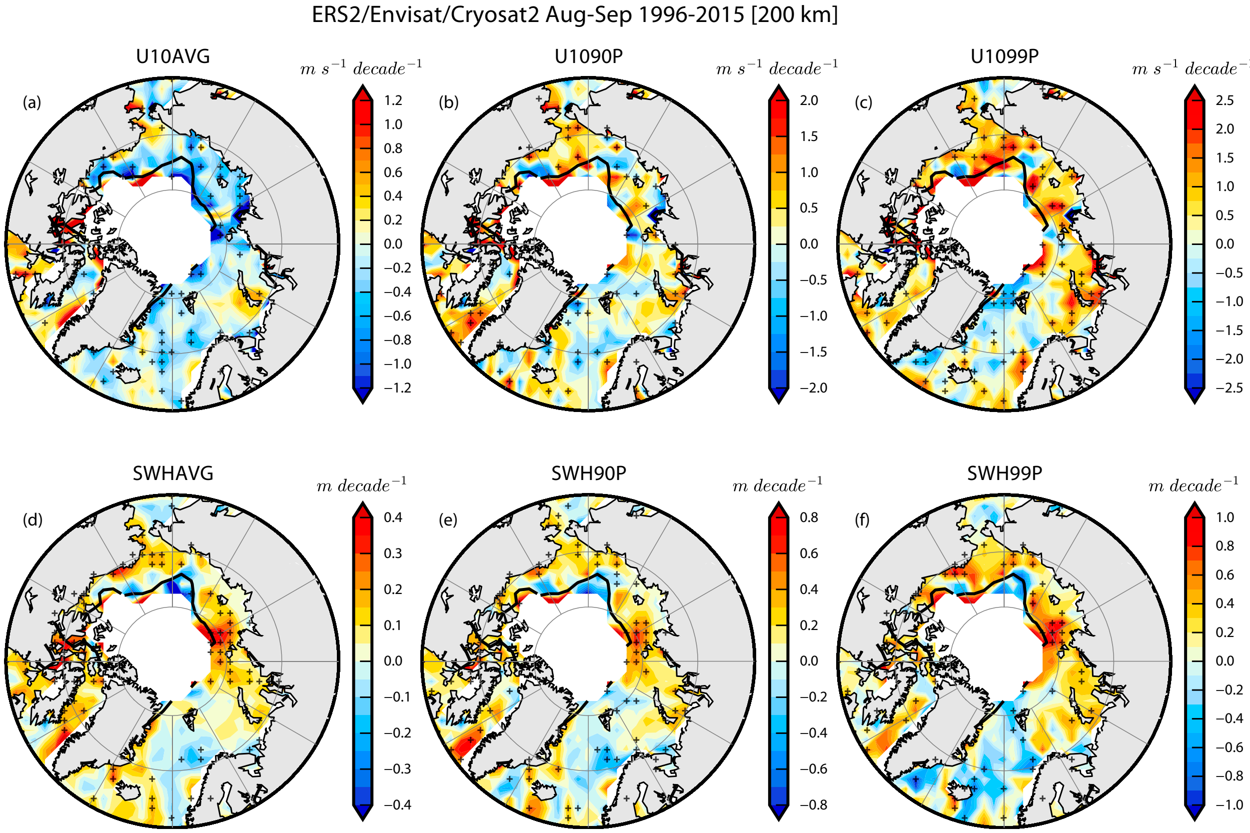

FIG. 7. Trend estimates (Sen's slope) of (a)–(c) wind speed ($\mathrm{m\,s^{-1}\,decade^{-1}}$) and (d)–(f) wave height ($\mathrm{m\,decade^{-1}}$) in Arctic Ocean. Markers (plus signs) indicate statistically significant trends at the 90% level.

Wallace 2012; Belleflamme et al. 2015), which, to some degree, explained the abrupt climate change in the Arctic over the recent years (Duarte et al. 2012). Undoubtedly, winds over the Arctic Ocean should have also changed somewhat due to changes of the large atmospheric circulations. Since wind generates waves, a question is then consequently raised to us: How have the waves in the Arctic Ocean varied as a response of this new climate regime? In an attempt to answer this question, we divided the duration of our altimeter data (1996–2015) into two separate periods, namely one period from 1996 through 2006 and the other one for the remaining years (2007–15). As seen in Figs. 6 and 7, winds and waves also characterize an apparent regional variability. Therefore, each separate subregion of the Arctic Ocean, as defined in Fig. 1, is also analyzed in detail, based on its regional average of the mean and 90th and 99th percentiles. Furthermore, the sea ice extent, expressed as the area proportion of open water, first-year ice, and multiyear ice in each specific subregion, is also calculated from the NSIDC sea ice age data (section 2e) to illustrate its variation over the past 20 years.

Maps with trends of wind speed and wave height for the two subperiods are presented in Fig. 8. All regional changes are presented in Table 2 and Fig. 9. Because of the relatively short durations of the first and second periods (11 and 9 yr, respectively), we noticed that the MKT is somewhat sensitive to the first and last values in the time series (Zieger et al. 2014). The magnitude of trend obtained here (Fig. 8) is higher compared to those for the full time period (Fig. 7). Nonetheless, we only focus on the sign of these trends instead (i.e., whether the climate of wave height and wind speed changed in a consistent way in these two separate periods or not). For the first period (Figs. 8a,b), both winds and waves show an upward trend across the entire Arctic with the Barents and Kara Seas being statistically significant regions. The mean wind speed and wave height in these regions increased at a rate of $1\,\mathrm{m\,s^{-1}\,decade^{-1}}$ and $0.4\,\mathrm{m\,decade^{-1}}$ (see also Table 2). Similarly, the 90th and 99th percentiles of winds and waves also give the consistent patterns (not shown), featuring an increase almost everywhere. In the second period, however, the opposite trend was observed: wind speed and wave height appear to have decreased in the Atlantic sector

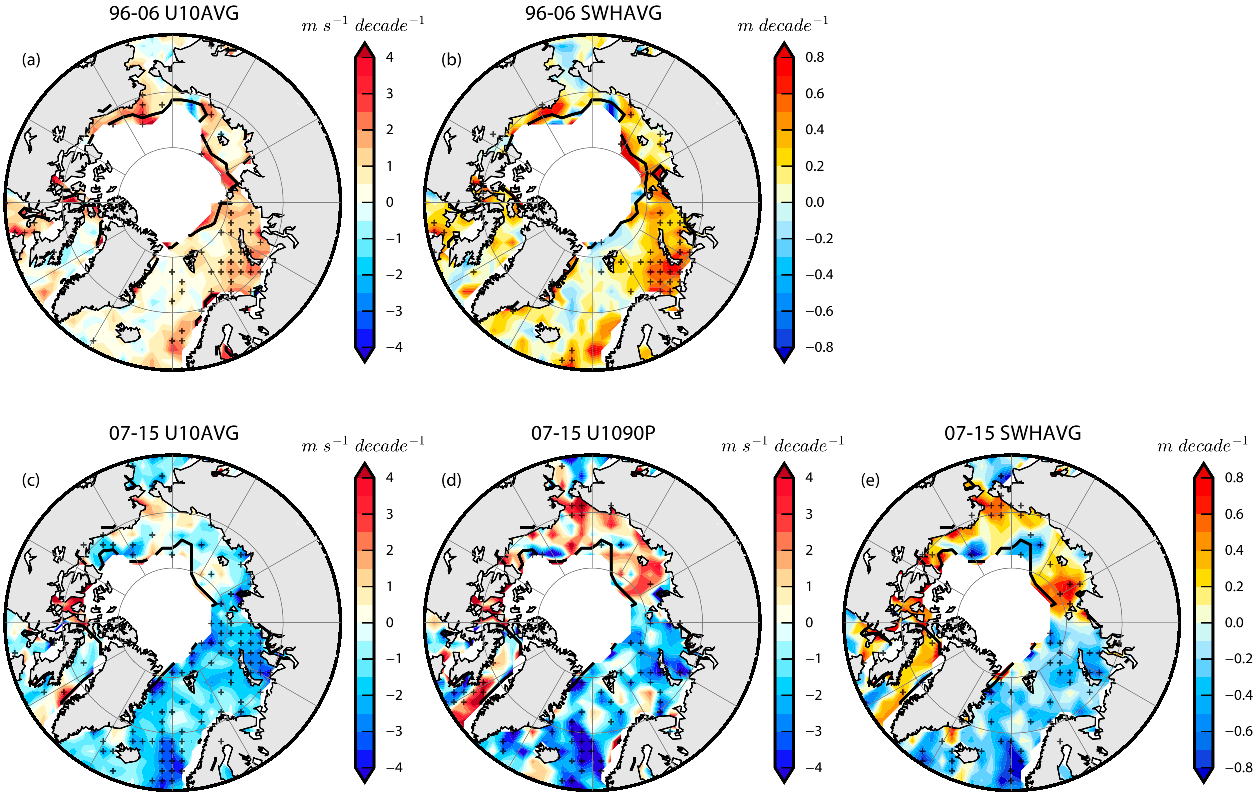

FIG. 8. Trend (Sen's slope) of summer wind speed (m s^{-1} decade^{-1}) and wave height (m decade^{-1}) in the Arctic Ocean for (top) the first period 1996–2006 and (bottom) the second period 2007–15. Black curves in the panels highlight the contour line of 8 and 6 sampling years, respectively. Each panel illustrates different statistics: (a),(c) for the average of U_{10}, (b),(e) for the average of H_s, and (d) for the 90th percentile of U_{10}.

(Figs. 8c–e). The mean wind speed decreased at a rate of around 2 m s^{-1} decade^{-1} or even higher in the Norwegian Sea and the southern Kara Sea. In contrast, some regions in the Chukchi and Laptev Seas still show an upward trend for wind speed, although it is not statistically significant. The 90th percentile of wind speed (Fig. 8d) presents an almost identical pattern except that the upward trend in the Chukchi and Laptev Seas is more pronounced. Wind speed over the eastern Baffin Bay is getting higher as well. The 99th percentile of wind speed and all the statistics of wave height generally give a very similar pattern as seen in Fig. 8d. Hence only trends of mean H_s are illustrated in Fig. 8e, which shows the average sea state in the southern Chukchi Sea and Laptev Sea has roughened at a rate of ~0.5 m decade^{-1}. The noticeable difference between these two periods (Figs. 8a,b vs Figs. 8c–e) is the limited open-ocean area in the Pacific sector (the Chukchi, Beaufort, and East Siberian Seas) in the first period. In these cases, the free ocean surface was limited to coastal regions around 70°N due to the presence of sea ice (Figs. 8a,b; see also Fig. 9a).

Figure 9 provides more details on the regional average time series of wind speed and wave height. For brevity, only four representative regions are included here: the Chukchi Sea (Fig. 9a), Laptev Sea (Fig. 9b), Kara Sea (Fig. 9c), and Barents Sea (Fig. 9d). An evident feature of these yearly time series is their large interannual variability. For example, in the Barents Sea (Fig. 9d), the 99th percentile of H_s reached its maximum (~5 m) in 2010 and then experienced a sharp drop to its minimum (~2.5 m) in 2011, after which a gradual recovery occurred in the successive years. In some regions, wind speed or wave height changed in a consistent way over the two subperiods, for instance, the mean H_s in the Laptev Sea shows a 0.23 m decade^{-1} increase in each subperiod, whereas in other regions like the Kara Sea (Fig. 9c) the variations of waves and winds behave like a decadal oscillation. Besides, there is a clear signature of the sea ice variability in the time series of winds and waves, especially for the first period (before 2007) in which the wave growth across the Arctic Shelf was generally limited by a greater sea ice extent (Figs. 9a–c). The local maximum open-ocean area frequently

TABLE 2. Regional trends of significant wave height (m decade^{-1}) and wind speed (m s^{-1} decade^{-1}) in the Arctic Ocean for average (AVG), 90th percentile (90P), and 99th percentile (99P) values. Significant trends at 90% level are highlighted in boldface text. Estimates in italics were calculated over the entire period 1996–2015 rather than the subperiods 1996–2006 and 2007–15. A spatial plot with the extent of the eight Arctic regions is given in Fig. 1.

	SWHAVG			SWH90P			SWH99P			U10AVG			U1090P			U1099P		
	96–06	07–15	*96–15*	96–06	07–15	*96–15*	96–06	07–15	*96–15*	96–06	07–15	*96–15*	96–06	07–15	*96–15*	96–06	07–15	*96–15*
Chukchi	0.04	0.09	***0.10***	0.09	0.32	***0.09***	0.21	0.46	***0.24***	**1.07**	−0.19	***0.18***	0.93	0.11	***0.46***	0.37	0.94	*0.50*
Beaufort	0.41	−0.05	*0.11*	0.59	**−0.12**	*0.19*	0.59	−0.28	*0.31*	1.67	**−1.48**	*−0.12*	2.56	−1.05	*0.04*	2.64	−1.43	*0.28*
E. Siberian	**0.41**	0.01	***0.14***	**0.56**	0.12	***0.24***	**0.97**	0.08	*0.40*	0.97	−0.67	***−0.17***	1.13	0.59	*0.08*	**2.21**	0.66	***0.82***
Laptev	**0.23**	**0.23**	***0.19***	0.32	**0.65**	***0.33***	0.19	**1.26**	***0.54***	0.74	**−1.18**	*−0.24*	0.78	0.73	***0.29***	0.75	**1.83**	***0.96***
Kara	**0.39**	**−0.23**	***0.14***	**0.49**	**−0.32**	***0.23***	**0.71**	−0.58	***0.31***	**1.37**	**−2.32**	*−0.04*	**2.22**	**−2.36**	*0.57*	**2.27**	−3.14	***1.07***
Barents	**0.26**	**−0.28**	*0.00*	**0.47**	−0.41	*−0.02*	**0.85**	0.33	*0.20*	**0.87**	**−1.47**	*−0.01*	**1.51**	**−1.49**	***0.18***	**2.02**	−1.11	*0.29*
Greenland	0.00	**−0.27**	*0.04*	0.26	−0.64	*0.01*	0.53	−0.84	*−0.17*	−0.03	**−1.77**	*−0.19*	0.22	**−2.28**	*0.00*	0.56	**−2.52**	*−0.35*
Baffin Bay	0.10	**0.17**	***0.13***	0.08	0.57	***0.30***	−0.12	0.09	***0.40***	0.20	**−0.52**	*−0.01*	−0.47	0.75	***0.53***	0.05	0.10	***0.70***

corresponds well with the occurrences of local extrema of wave height and wind speed, particularly for the 90th and 99th percentiles (see, e.g., Figs. 9b,c). Two factors contributed to these coincidences. First, the more (less) open ocean area we have, the better (less well) altimeters can detect extreme high or low events, mainly because we integrate all values across each subregion. This also explains why ice has such an obvious effect on wind speed (over the open ocean). Second, the physical influence of ice on wave evolution in the Arctic, such as fetch, defines the size of the wind sea in the region (Khon et al. 2014; Wang et al. 2015). The simulations of future wave climate change in the Arctic showed that the ice retreat contributes more than 70% variability of waves in the Arctic Shelf seas such as the the Chukchi, East Siberian, and Laptev Seas (Khon et al. 2014). Wang et al. (2015) reached a consistent conclusion that changes of wind speed alone cannot explain the significant trends of wave height from their Beaufort–Chukchi reanalysis data. Our measurements in the Chukchi Sea, however, show a statistically significant increase in both wind speed and wave height (0.18 m s^{-1} decade^{-1} and 0.1 m decade^{-1}, respectively; Table 2) and therefore we cannot draw the same conclusion unambiguously. Nonetheless, an evident manifestation of these arguments is seen in the Laptev Sea (Fig. 9b): in the second period, wind speed over this region declined significantly (−1.18 m s^{-1} decade^{-1}) while wave height increased simultaneously (0.23 m decade^{-1}) because of the dramatic retreat of sea ice and the increasing extreme winds. It should be noted that, in the Atlantic sector, such as the Barents Sea, this is of course not the case because this region is almost ice-free everywhere in summer (Fig. 9d). Local winds and remotely generated swell combine together to determine changes of sea state in these regions (e.g., Semedo et al. 2015; Dobrynin et al. 2014).

4. Discussion

a. Comparison with ERA-Interim

A recent model study by Dobrynin et al. (2012) found that within the framework of their Earth system model (EC-Earth; Hazeleger et al. 2012), the 3G spectral wave model (WAM; Hasselmann et al. 1988; Janssen 2004) underestimated H_s by 0.3–0.4 m in comparison to altimeter observations in the Arctic Ocean (their Fig. S1). Dobrynin et al. (2012) suggested that the poor agreement between model and data was most likely due to the sparse coverage at high latitudes by altimeter. However, many factors can cause mismatch between numerical wave models and measurements. It is better to analyze such

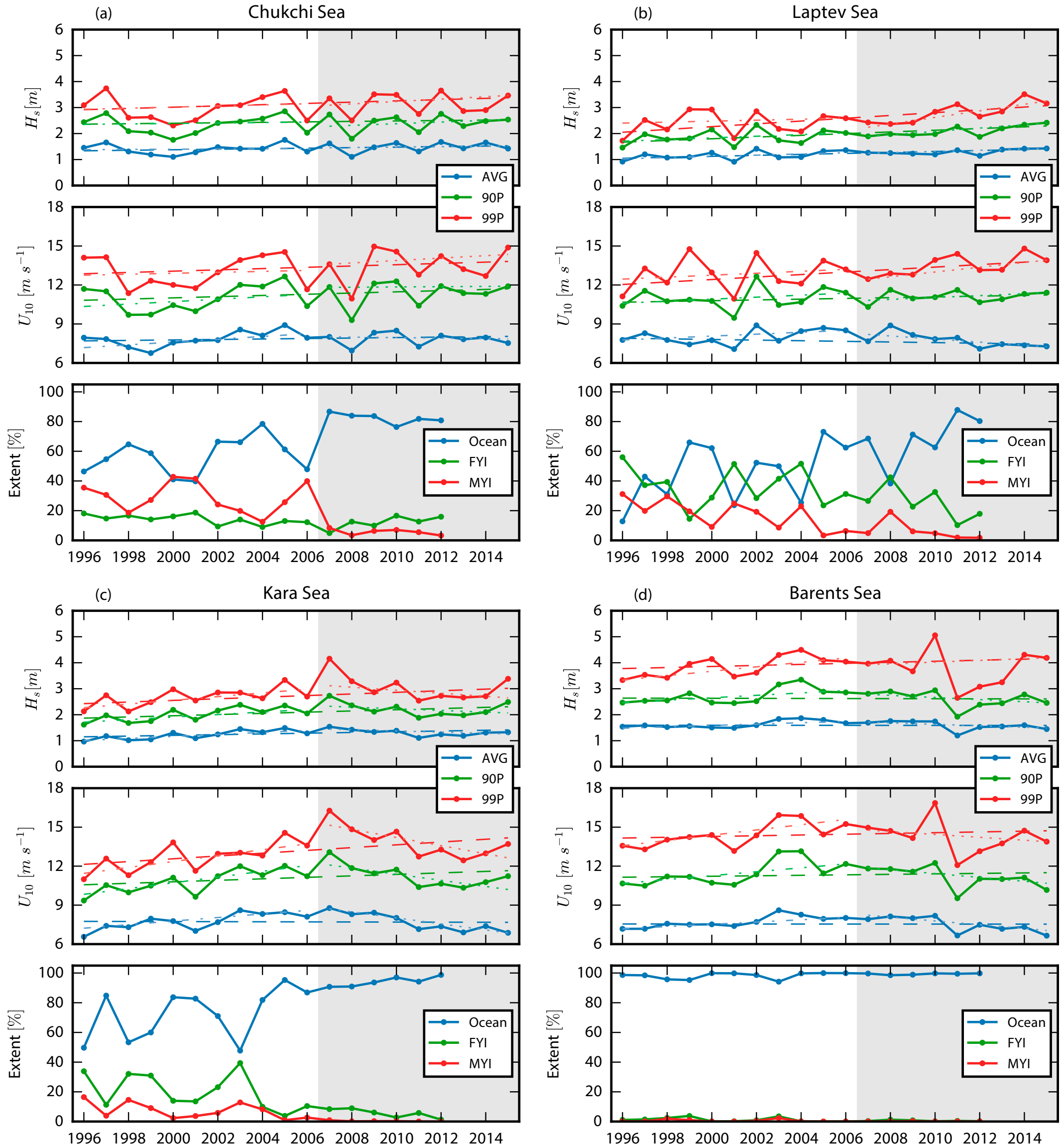

FIG. 9. The regional mean time series of wind speed and wave height in the (a) Chukchi, (b) Laptev, (c) Kara, and (d) Barents Seas. Each panel consists of three plots, presenting the variation of H_s (m), U_{10} (m s^{-1}), and sea ice extent (%), respectively. In the top two plots of each panel, the terms AVG, 90P, and 99P respectively denote the average and 90th and 99th percentiles. Trends for the whole duration (1996–2015; dashed line), the first period (1996–2006; dashed-dotted line), and the second period (2007–15; dotted line) are also presented. The sea ice extent over 1996–2012, as illustrated in the bottom plot of each panel, gives the area proportion of the open water (Ocean), first-year ice (FYI), and multiyear ice (MYI) in each specific subregion. For clarity, the second period (2007–15) is gray shaded in each panel.

incompatibility in a more prudent way. EC-Earth used by Dobrynin et al. (2012) shares a number of similarities with the ECMWF Integrated Forecast System (IFS) that produces the reanalysis dataset ERA-Interim (hereinafter ERAI; Dee et al. 2011; Hazeleger et al. 2012). Here for generality, we compared our altimeter data with the 6-hourly, 0.75° ERAI dataset rather than the model output from Dobrynin et al. (2012). For consistency, the original ERAI data were also binned into $200 \times 200\,\text{km}^2$ bins in the same way as we processed altimeter data (see section 2c). No collocation procedures between ERAI and altimeters were applied.

Figure 10 shows the comparison for wind speed (Figs. 10a–c) and wave height (Figs. 10d–f). The spatial patterns obtained from ERAI agree well with the altimeter-derived ones (Figs. 6a,d). However, when comparing

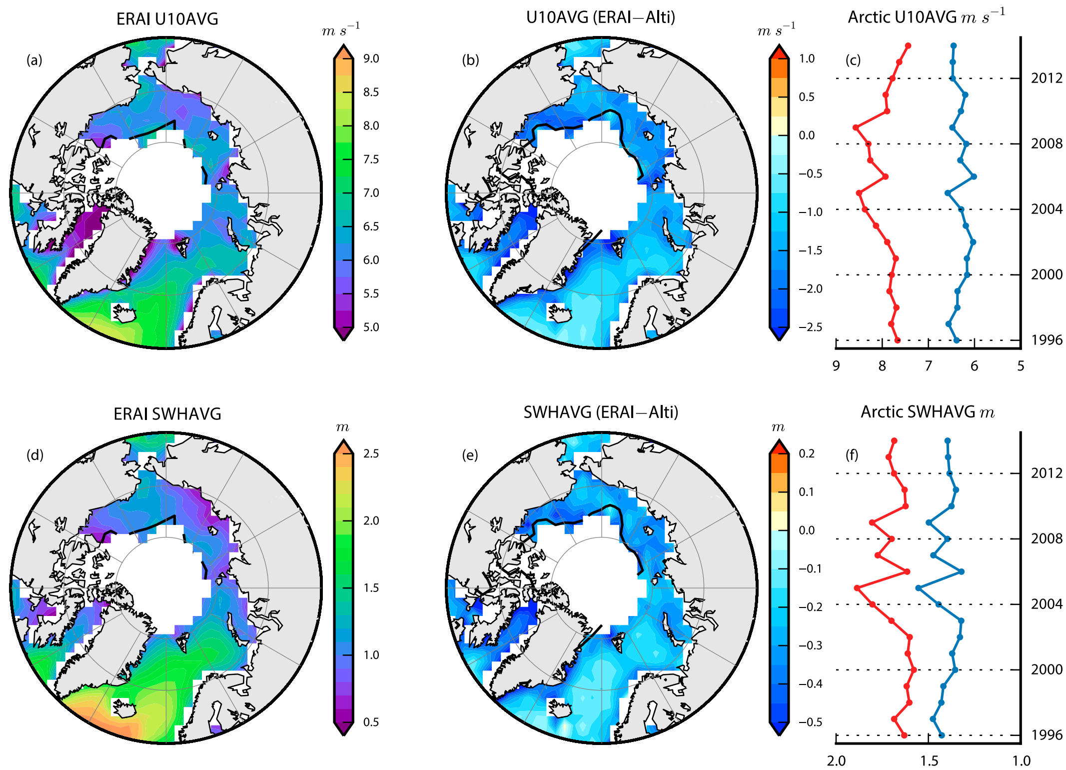

FIG. 10. Comparison of (top) mean wind speed U_{10} (over waves) and (bottom) wave height H_s between ERAI and altimeter measurements over the period from 1996 to 2014: (a) ERAI U_{10}, (b) ERAI U_{10} minus altimeter U_{10}, (c) yearly time series of ERAI U_{10} (blue line) vs altimeter U_{10} (red line) with a bias of $-1.64\,\mathrm{m\,s^{-1}}$, (d) ERAI H_s, (e) ERAI H_s minus altimeter H_s, and (f) yearly time series of ERAI H_s (blue line) vs altimeter H_s (red line) with a bias of -0.27 m. Note that for consistency, ERAI data were binned into 200-km cells in the same way as we processed altimeter measurements. The black curves denote the contour line of 10 sampling years by ERAI in (a) and (d) and by altimeter in (b) and (e).

magnitudes of ERAI U_{10} and H_s with altimeter data, an obviously negative bias was found (Figs. 10b,e). This suggests that across the Arctic Ocean ERAI winds and waves are systematically underestimated, especially for the Arctic Shelf. Yearly ERAI U_{10} and H_s time series (Figs. 10c,f) show an overall bias of $-1.64\,\mathrm{m\,s^{-1}}$ and -0.27 m relative to altimeter data. There exist a number of factors that can lead to such underestimation of H_s in the wave model: 1) the performance of wave models in the Arctic, whether this is physics of existing source terms, or wave–ice interactions, or wave fetches (due to, e.g., uncertain ice cover), 2) quality of forcing fields (e.g., winds, ice, and currents), and 3) quality of altimeter data. As shown in Fig. 10, the contour lines of 10 sampling years by ERAI (Figs. 10a,c) and altimeter values (Figs. 10d,f) deviate from each other. This is because 1) the WAM model in the ECMWF IFS does not allow waves to propagate in the areas with ice concentration above 30% (Doble and Bidlot 2013) and 2) there should be potential errors in both ERAI and the altimeter-estimated ice cover (see section 2). Nonetheless, since ERAI winds and waves are simultaneously underestimated, we argue that the poor performance of WAM in the Arctic, as reported in Dobrynin et al. (2012), is probably because of the biased wind forcing. The assimilation of wave measurements from *ERS-2* and *Envisat* in the ERAI (Dee et al. 2011) was not capable to fully correct the negative bias in H_s resulted from the lower wind forcing in the Arctic Ocean. Hughes and Cassano (2015) analyzed different reanalyses in the pan-Arctic area and found that ERAI winds are slightly weaker compared with other reanalyses such as NCEP's Climate Forecast System Reanalysis (CFSR), which partially supports our conclusions (see their Figs. 2 and 5). Francis et al. 2016, manuscript submitted to *J. Geophys. Res.*) also showed that ERAI underestimated wind speed in the Chukchi Sea when compared with scatterometer measurements from QuikScat, agreeing well with our arguments here. A detailed intercomparison between winds from different reanalyses and altimeter measurements in the Arctic Ocean, however, is beyond the scope of this paper. It should be noted that the underestimation of U_{10} by ERAI in the Arctic found here is consistent with the behavior of ERAI in the global basin, as revealed by the study of Stopa and Cheung (2014).

b. Large-scale atmospheric circulation

In the Barents Sea, the mean U_{10} and H_s values suddenly dropped in 2011 (Fig. 9d), with a decrease in H_s of about 0.5 m and in U_{10} of about 1.5 m s^{-1}. This behavior is more pronounced when looking at the 99th percentile U_{10} and H_s values. Interestingly, ERAI reanalysis also supports such drop in the mean values. So how can one explain such a drop in wind speed and wave height? The atmospheric circulation in the Arctic Ocean is quite complex and a number of large-scale modes can affect this particular region. A very good introduction of this topic can be found in Serreze and Barry (2014, ch. 4). Following Wang et al. (2009), we focused on two main modes, namely the Arctic Oscillation (AO, also known as the northern annular mode; Thompson and Wallace 1998) and the Arctic dipole anomaly (AD; Wang et al. 2009; Overland et al. 2012), which are very important for the Arctic Ocean in summer. The AO refers to an annular sea level pressure (SLP) anomaly over the entire Arctic. During its positive (negative) phase, the Arctic shows below (above) normal SLP, an enhanced (weaken) polar circulation, and a cyclonic (anticyclonic) wind anomaly. In contrast to the AO, the AD-driven SLP anomaly has two action centers in the Arctic. We note that the definition of the AD index in Overland et al. (2012) is adopted here, which is opposite in sign to the one proposed by Wang et al. (2009). A negative (positive) AD phase features a higher (lower) SLP on the North American side of the Arctic and lower (higher) SLP on the Siberian side. During 1996–2015, the AO index is relatively neutral (black line with dots in Fig. 12c). However, the AD index shows slightly more variability and its maximum (2.35) appeared in September 2011 (red bar in Fig. 12d), which is coherent with the abnormal behavior of the altimeter data in this year. Figure 11 shows the SLP anomalies for the years 2010 and 2011 as referenced to 1996–2015 climatology for the months August and September. By convention, SLP anomalies are calculated from the NCEP–NCAR reanalysis dataset (Kalnay et al. 1996). Figure 11a shows a negative AD mode in 2010 whereas in 2011 the AD index became positive (Figs. 11b and 12d). The switch in the phase of AD from 2010 to 2011 may be the driver for the sharp decline in U_{10} and H_s in the Barents Sea (Fig. 9d). In 2011, the higher SLP over the Barents Sea potentially blocked the penetration of the southerly and southwesterly storms from the North Atlantic track and also influenced the cyclogenesis in this region, resulting in a lower than average wind speed and wave height.

To investigate the correlations between the changes of altimeter measured winds (and waves) and the two large-scale modes further, we performed an empirical orthogonal function (EOF) analysis (Wilks 2006) on our altimeter data. Figures 12a and 12b show the first two leading EOF modes calculated for the mean wind speed. Note that the EOF algorithm cannot handle missing values, so only grid points with 20 years of data were analyzed. As a consequence, our data are mainly restricted to the Atlantic sector. The first EOF mode (EOF1; Fig. 12a) accounts for 19% of the total variance and is formed by the anomalies of one sign on the entire Atlantic side, characterizing an AO-like pattern [see Fig. 2c of Wang et al. (2009)]. The corresponding normalized principal component (PC1) correlates well with the AO index with a correlation coefficient R of 0.66 (Fig. 12c). The second EOF mode (EOF2; Fig. 12b) accounts for 9% of the total variance and is characterized by the anomalies of one sign in the Greenland Sea and the anomalies of the opposite sign in the Barents and Kara Seas. This shares some similarity with the AD mode [see Fig. 2d of Wang et al. (2009), and also Fig. 11b herein]. Surprisingly, the correlation between the second PC (PC2) and the AD index is as low as 0.32 (Fig. 12d). The PC2 is negatively correlated with the AD index ($R = -0.33$) during the period 1996–2005; over the last decade (2006–15), a high correlation ($R = 0.77$) between the AD index and the PC2 is found. It is not clear what caused the negative correlation in the earlier period. The AD pattern is formally defined as the second EOF of SLP anomaly north of 70°N (Overland et al. 2012), which is based on NCAR–NCEP reanalysis dataset. While the altimeter-derived modes (Figs. 12a,b) are limited to north of 60°N with the data for the central Arctic totally absent. The differences in the areal extent of altimeter data and reanalysis should contribute to the mismatch between the PC2 and the AD index. Other possible factors are open to question. Nonetheless, as we discussed above, the AO and AD modes have clear signatures in the changes of U_{10} in the Arctic Ocean. The EOF analysis applied on the mean H_s (not shown), however, shows fewer effects of these two modes ($R = 0.52$ between the AO index and PC1 and $R = 0.04$ between the AD index and PC2), indicating that other factors like remotely generated swell play an additional role particularly in the Atlantic sector (Semedo et al. 2015; Stopa et al. 2016b).

5. Conclusions

Twenty years (1996–2015) of altimeter measurements, across three satellite missions (*ERS-2*, *Envisat*, and *CryoSat-2*), were analyzed to study the climatology and trends of the oceanic winds and waves in the Arctic Ocean in summer season (August–September). Altimeter records

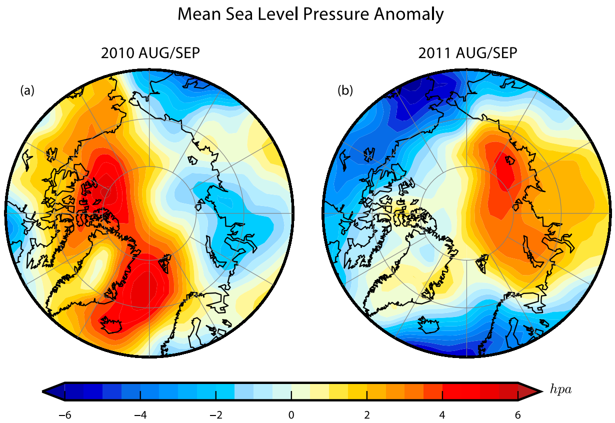

FIG. 11. Anomalies in mean SLP as referenced to 1996–2015 climatology for the summer (August and September) of (a) 2010 and (b) 2011, based on the NCEP–NCAR reanalysis.

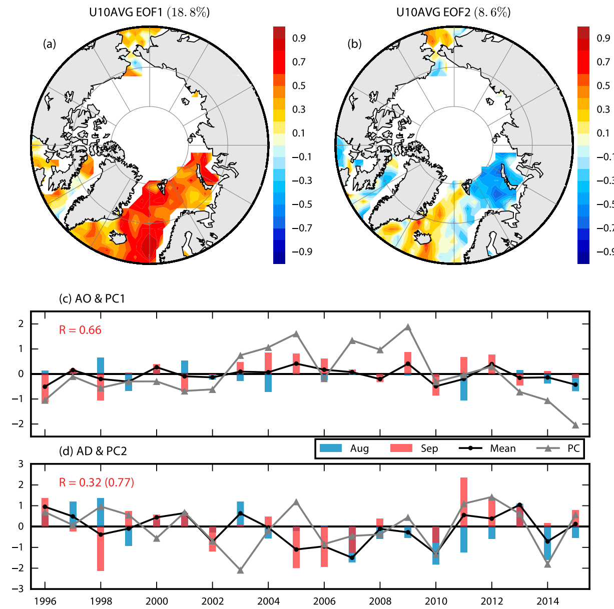

FIG. 12. (a),(b) The two leading EOF modes (variance in parentheses) of wind speed anomalies in the Arctic Ocean as observed by altimeter over 1996–2015 summer months. (c) The PC1 (gray line with triangles), together with the monthly AO index (August is blue bars; September is red bars; and the 2-month average is the black line with dots). The correlation coefficient R between PC1 and the 2-month average of the AO index is also printed in the top-left corner. (d) The PC2 and AD index.

contaminated by sea ice were identified and eliminated by adopting an universal one-parameter mapping algorithm, first validated by means of the three-parameter approach (Fig. 4). Calibrated and validated estimates of wind speed (U_{10}) and wave height (H_s) were averaged over 200 × 200 km^2 bins (Fig. 5) to compute the climatological statistics (average and 90th and 99th percentiles) and to investigate their spatial and temporal variability. To analyze the regional variability, the Arctic Ocean was subdivided into eight geographic regions (Fig. 1) by using the regional mask developed by Parkinson et al. (1999) and Meier et al. (2007). Our main findings can be summarized as follows.

In summer (August and September), the Arctic Ocean shows an average U_{10} around 8 m s^{-1} (Figs. 6a and 10c). The maximum of the average U_{10} appears in the south of Iceland due to the Icelandic low and the North Atlantic storm track; the minimum average U_{10} is presented in the central East Siberian Sea and the northern Baffin Bay. The extreme U_{10} (90th and 99th percentiles; Figs. 6b,c) is highest in the Denmark Strait due to the strong barrier jets along the southeast coast of Greenland (Harden et al. 2011; Harden and Renfrew 2012; Hughes and Cassano 2015). The sea state (mean H_s) in the Arctic features an average of 1.7 m (Figs. 6d and 10f). Waves in the Atlantic sector are generally more energetic than those in the Pacific sector due to the higher wind speed and the penetration of remotely generated swell (e.g., Stopa et al. 2016b). The minimum wave height (about 1 m) is presented in the southern East Siberian Sea because of the relatively low winds and the limited fetch. As a response to the strong barrier jets, the peak values of the extreme H_s (99th percentile) also appear in the Denmark Strait (Fig. 6f).

The trend (Sen's slope) of the average U_{10} in the summer Arctic is mainly dominated by a negative sign (Fig. 7a). This is very clear in the East Siberian, Laptev, and Greenland Seas (≥0.4 m s^{-1} decade^{-1}). Positive trends can be found in regions west and north of the Alaskan coast, around the Novaya Zemlya archipelago and in the southern Baffin Bay. The changes of U_{10} in the Atlantic sector, computed from the altimeter observations, agree well with Stopa et al. (2016b). In the Chukchi, East Siberian, and Laptev Seas, there are however some inconsistencies between our results and those estimated from reanalyses (Wang et al. 2015; Stopa et al. 2016b), which might need further research. Extreme winds (99th percentile) have generally increased in the Arctic with the exception of the Greenland and Barents Seas (Figs. 7b,c), indicating storms may have become more frequent in the Arctic Shelf seas over the last two decades. This is consistent with the findings reported in Sepp and Jaagus (2011). Several regions of the Arctic with positive trends in H_s (average and 90th and 99th percentiles) have been identified in our study (Figs. 7d–f), including the western Beaufort Sea, the Chukchi Sea, the Laptev Sea, the Kara Sea, and Baffin Bay. Among these regions, the Laptev Sea and the western Beaufort–Chukchi Seas (especially near the north coast of Alaska) characterize the highest upward trends (>0.3 m decade^{-1}). In the Laptev Sea, it is very clear that although the average wind speed decreased in 2007–15, the wave height still increased because of the increase of the effective fetch (less ice cover) and the increasing extreme winds (99th percentile; Fig. 9b).

Except the clear regional variability, the U_{10} and H_s in the summer Arctic also presented apparent interannual variability. In the Barents and Kara Seas, winds and waves increased in the period 1995–2006 and then decreased in the successive years (2007–15) (Figs. 8 and 9c,d). The Arctic Oscillation (AO) is proved to influence the changes of U_{10} ($R = 0.66$; Fig. 12) and the Arctic dipole anomaly (AD) is helpful to explain the abrupt decrease in U_{10} and H_s in 2011, as observed by altimeters. The two large atmospheric modes (AO and AD) showed less effects on wave height in the Atlantic sector, suggesting that other factors such as swell influence this region (Semedo et al. 2015).

Our study also found that in the Arctic the reanalyzed U_{10} from ERAI is 1.6 m s^{-1} lower than the altimeter measurements, and as a result the reanalyzed H_s from ERAI is 0.27 m lower than the altimeter-estimated wave height. An accurate description of U_{10} is crucial to correctly determine the momentum flux at the air–sea ice interface. The potential limitation of the ERAI data should be kept in mind when ERAI U_{10} is applied to force numerical wave, current, and ice models (e.g., Thomson et al. 2016).

Finally, to sum up, in the two regions that show clear increasing wave height, namely the Laptev Sea and the western Beaufort–Chukchi Seas, extreme winds (storms) are increasing and the effective fetch is becoming larger because of the ice retreat. Wang et al. (2015) showed the regional mean of the mean wave period in the Beaufort–Chukchi–Bering Seas has more than tripled since 1970. The increasing of the wave period in the Laptev Sea is also revealed by Stopa et al. (2016b). All these environmental changes favor an increasing wave energy flux and therefore an intensified wave ice–coast interaction. The research by Thomson et al. (2016) suggested that the increasing wave energy in the Beaufort and Chukchi Seas preferentially directed toward the Alaskan coast [see also Overeem et al. (2011)]. In the Laptev Sea, the prevalent waves propagates northward to the ice cover (Stopa et al. 2016b). Therefore, it is likely that the wave energy flux arriving at the ice edge in the Laptev Sea is becoming more and more important to fracture the ice floes and pack. In addition, as our reviewer pointed out, August–September is a limit view of the climate. Wave–ice interaction may be more critical in October and November, when there is still ice-free water and coincident stronger wind speeds [e.g., see Fig. 12 of Thomson et al. (2016) and Fig. 13 of Stopa et al. (2016b)]. A comprehensive coupled air–wave–ice–ocean model framework is necessary to quantify the complex ice–wave feedback. Dedicated field measurements and observation- and/or physics-based theories of waves coupled with ice are also crucial to understand this complicated topic (Thomson et al. 2013).

Acknowledgments. Q. Liu acknowledges the fellowship supported by China Scholarship Council (CSC; 201406330003). The authors are thankful for all comments and criticism raised by three independent reviewers. The ERA-Interim, NCEP–NCAR reanalyses, and EASE-Grid sea ice age data were kindly provided by the ECMWF, U.S. NOAA/ESRL PSD, and U.S. NSIDC, respectively. The AO index is sourced from the U.S. NCEI. We appreciate Dr. Walter Meier and Dr. Julienne Stroeve providing us the subregion masks of the Arctic Ocean. We also acknowledge Dr. Muyin Wang and Dr. James Overland for providing us their monthly AD index. AVB acknowledges support from the Australian Research Council Discovery Grant DP130100227 and the U.S. Office of Naval Research Grant N00014-13-1-0278. C. Guan appreciates the support from the National Natural Science Foundation of China (Grants 41276010 and U1406401).

REFERENCES

Abdalla, S., 2012: Ku-band radar altimeter surface wind speed algorithm. *Mar. Geod.*, **35**, 276–298, doi:10.1080/01490419.2012.718676.

Ardhuin, F., and Coauthors, 2010: Semi-empirical dissipation source functions for ocean waves. Part I: Definition, calibration, and validation. *J. Phys. Oceanogr.*, **40**, 1917–1941, doi:10.1175/2010JPO4324.1.

Babanin, A. V., 2011: *Breaking and Dissipation of Ocean Surface Waves.* Cambridge University Press, 480 pp.

——, S. Zieger, and A. Ribal, 2014: Satellite observations of waves in the Arctic Ocean. *Proc. 22nd IAHR Int. Symp. on Ice*, Singapore, International Association of Hydro-Environment Engineering and Research, 798–805.

Belleflamme, A., X. Fettweis, and M. Erpicum, 2015: Recent summer Arctic atmospheric circulation anomalies in a historical perspective. *Cryosphere*, **9**, 53–64, doi:10.5194/tc-9-53-2015.

Bernier, N. B., and Coauthors, 2016: Operational wave prediction system at Environment Canada: Going global to improve regional forecast skill. *Wea. Forecasting*, **31**, 353–370, doi:10.1175/WAF-D-15-0087.1.

Brodzik, M. J., B. Billingsley, T. Haran, B. Raup, and M. H. Savoie, 2012: EASE-Grid 2.0: Incremental but significant improvements for Earth-gridded data sets. *ISPRS Int. J. Geoinf.*, **1**, 32–45, doi:10.3390/ijgi1010032.

Caires, S., A. Sterl, J.-R. Bidlot, N. Graham, and V. Swail, 2004: Intercomparison of different wind wave reanalyses. *J. Climate*, **17**, 1893–1913, doi:10.1175/1520-0442(2004)017<1893:IODWR>2.0.CO;2.

Cavaleri, L., B. Fox-Kemper, and M. Hemer, 2012: Wind waves in the coupled climate system. *Bull. Amer. Meteor. Soc.*, **93**, 1651–1661, doi:10.1175/BAMS-D-11-00170.1.

Chelton, D. B., J. C. Ries, B. J. Haines, L.-L. Fu, and P. S. Callahan, 2001: Satellite altimetry. *Satellite Altimetry and Earth Sciences: A Handbook of Techniques and Applications*, L.-L. Fu and A. Cazenave, Eds., International Geophysics Series, Vol. 69, Academic Press, 1–133.

Collins, C. O., W. E. Rogers, A. Marchenko, and A. V. Babanin, 2015: In situ measurements of an energetic wave event in the Arctic marginal ice zone. *Geophys. Res. Lett.*, **42**, 1863–1870, doi:10.1002/2015GL063063.

Comiso, J. C., and F. Nishio, 2008: Trends in the sea ice cover using enhanced and compatible AMSR-E, SSM/I, and SMMR data. *J. Geophys. Res.*, **113**, C02S07, doi:10.1029/2007JC004257.

Dee, D. P., and Coauthors, 2011: The ERA-Interim reanalysis: Configuration and performance of the data assimilation system. *Quart. J. Roy. Meteor. Soc.*, **137**, 553–597, doi:10.1002/qj.828.

Doble, M. J., and J. R. Bidlot, 2013: Wave buoy measurements at the Antarctic sea ice edge compared with an enhanced ECMWF WAM: Progress towards global waves-in-ice modelling. *Ocean Modell.*, **70**, 166–173, doi:10.1016/j.ocemod.2013.05.012.

Dobrynin, M., J. Murawski, and S. Yang, 2012: Evolution of the global wind wave climate in CMIP5 experiments. *Geophys. Res. Lett.*, **39**, L18606, doi:10.1029/2012GL052843.

——, ——, J. Baehr, and T. Ilyina, 2014: Detection and attribution of climate change signal in ocean wind waves. *J. Climate*, **28**, 1578–1591, doi:10.1175/JCLI-D-13-00664.1.

Duarte, C. M., T. M. Lenton, P. Wadhams, and P. Wassmann, 2012: Abrupt climate change in the Arctic. *Nat. Climate Change*, **2**, 60–62, doi:10.1038/nclimate1386.

Francis, O. P., G. G. Panteleev, and D. E. Atkinson, 2011: Ocean wave conditions in the Chukchi Sea from satellite and in situ observations. *Geophys. Res. Lett.*, **38**, L24610, doi:10.1029/2011GL049839.

Frey, K. E., G. W. K. Moore, L. W. Cooper, and J. M. Grebmeier, 2015: Divergent patterns of recent sea ice cover across the Bering, Chukchi, and Beaufort Seas of the Pacific Arctic region. *Prog. Oceanogr.*, **136**, 32–49, doi:10.1016/j.pocean.2015.05.009.

Gulev, S. K., and V. Grigorieva, 2006: Variability of the winter wind waves and swell in the North Atlantic and North Pacific as revealed by the voluntary observing ship data. *J. Climate*, **19**, 5667–5685, doi:10.1175/JCLI3936.1.

Hamed, K. H., and A. Rao, 1998: A modified Mann–Kendall trend test for autocorrelated data. *J. Hydrol.*, **204**, 182–196, doi:10.1016/S0022-1694(97)00125-X.

Harden, B. E., and I. A. Renfrew, 2012: On the spatial distribution of high winds off southeast Greenland. *Geophys. Res. Lett.*, **39**, L14806, doi:10.1029/2012GL052245.

——, ——, and G. N. Petersen, 2011: A climatology of wintertime barrier winds off southeast Greenland. *J. Climate*, **24**, 4701–4717, doi:10.1175/2011JCLI4113.1.

Hasselmann, S., and Coauthors, 1988: The WAM model—A third generation ocean wave prediction model. *J. Phys. Oceanogr.*, **18**, 1775–1810, doi:10.1175/1520-0485(1988)018<1775:TWMTGO>2.0.CO;2.

Hazeleger, W., and Coauthors, 2012: EC-Earth V2.2: Description and validation of a new seamless Earth system prediction model. *Climate Dyn.*, **39**, 2611–2629, doi:10.1007/s00382-011-1228-5.

Hemer, M. A., J. A. Church, and J. R. Hunter, 2010: Variability and trends in the directional wave climate of the Southern Hemisphere. *Int. J. Climatol.*, **30**, 475–491, doi:10.1002/joc.1900.

Hirsch, R. M., J. R. Slack, and R. A. Smith, 1982: Techniques of trend analysis for monthly water quality data. *Water Resour. Res.*, **18**, 107–121, doi:10.1029/WR018i001p00107.

Hughes, M., and J. J. Cassano, 2015: The climatological distribution of extreme Arctic winds and implications for ocean and sea ice processes. *J. Geophys. Res. Atmos.*, **120**, 7358–7377, doi:10.1002/2015JD023189.

Janssen, P., 2004: *The Interaction of Ocean Waves and Wind.* Cambridge University Press, 300 pp.

Jeffries, M. O., J. E. Overland, and D. K. Perovich, 2013: The Arctic shifts to a new normal. *Phys. Today*, **66**, 35–40, doi:10.1063/PT.3.2147.

Kalnay, E., and Coauthors, 1996: The NCEP/NCAR 40-Year Reanalysis Project. *Bull. Amer. Meteor. Soc.*, **77**, 437–471, doi:10.1175/1520-0477(1996)077,0437:TNYRP.2.0.CO;2.

Kendall, M. G., 1955: *Rank Correlation Methods.* Griffin, 202 pp.

Khon, V. C., I. I. Mokhov, F. A. Pogarskiy, A. V. Babanin, K. Dethloff, A. Rinke, and H. Matthes, 2014: Wave heights in the 21st century Arctic Ocean simulated with a regional climate model. *Geophys. Res. Lett.*, **41**, 2956–2961, doi:10.1002/2014GL059847.

Laxon, S., 1990: Seasonal and inter-annual variations in Antarctic sea ice extent as mapped by radar altimetry. *Geophys. Res. Lett.*, **17**, 1553–1556, doi:10.1029/GL017i010p01553.

Liu, Q., A. V. Babanin, C. Guan, S. Zieger, J. Sun, and Y. Jia, 2016: Calibration and validation of HY-2 altimeter wave height. *J. Atmos. Oceanic Technol.*, **33**, 919–936, doi:10.1175/JTECH-D-15-0219.1.

Mann, H., 1945: Nonparametric tests against trend. *Econometrica*, **13**, 245–259, doi:10.2307/1907187.

Maslanik, J. A., C. Fowler, J. Stroeve, S. Drobot, J. Zwally, D. Yi, and W. Emery, 2007: A younger, thinner Arctic ice cover: Increased potential for rapid, extensive sea-ice loss. *J. Geophys. Res.*, **34**, L24501, doi:10.1029/2007GL032043.

——, J. Stroeve, C. Fowler, and W. Emery, 2011: Distribution and trends in Arctic sea ice age through spring 2011. *Geophys. Res. Lett.*, **38**, L13502, doi:10.1029/2011GL047735.

Meier, W. N., J. Stroeve, and F. Fetterer, 2007: Whither Arctic sea ice? A clear signal of decline regionally, seasonally and extending beyond the satellite record. *Ann. Glaciol.*, **46**, 428–434, doi:10.3189/172756407782871170.

Ogi, M., and J. M. Wallace, 2012: The role of summer surface wind anomalies in the summer Arctic sea ice extent in 2010 and 2011. *Geophys. Res. Lett.*, **39**, L09704, doi:10.1029/2012GL051330.

Overeem, I., R. S. Anderson, C. W. Wobus, G. D. Clow, F. E. Urban, and N. Matell, 2011: Sea ice loss enhances wave action at the Arctic coast. *Geophys. Res. Lett.*, **38**, L17503, doi:10.1029/2011GL048681.

Overland, J. E., J. A. Francis, E. Hanna, and M. Wang, 2012: The recent shift in early summer Arctic atmospheric circulation. *Geophys. Res. Lett.*, **39**, L19804, doi:10.1029/2012GL053268.

Parkinson, C. L., D. J. Cavalieri, P. Gloersen, H. J. Zwally, and J. C. Comiso, 1999: Arctic sea ice extents, areas, and trends, 1978–1996. *J. Geophys. Res.*, **104**, 20 837–20 856, doi:10.1029/1999JC900082.

Perovich, D. K., B. Light, H. Eicken, K. F. Jones, K. Runciman, and S. V. Nghiem, 2007: Increasing solar heating of the Arctic Ocean and adjacent seas, 1979–2005: Attribution and role in the ice–albedo feedback. *Geophys. Res. Lett.*, **34**, L19505, doi:10.1029/2007GL031480.

Rinne, E., and H. Skourup, 2012: Sea ice detection using *Envisat* radar altimeter 2. *Fall Meeting 2012*, San Francisco, CA, Amer. Geophys. Union, Abstract C21C-0618.

Rogers, W. E., and S. Zieger, 2014: New wave–ice interaction physics in WAVEWATCH III. *Proc. 22nd IAHR Intl. Symp. on Ice*, Singapore, International Association of Hydro-Environment Engineering and Research, 8 pp. [Available online at www7320.nrlssc.navy.mil/pubs/2014/rogers1-2014.pdf.]

Semedo, A., R. Vettor, Ø. Breivik, A. Sterl, M. Reistad, C. G. Soares, and D. Lima, 2015: The wind sea and swell waves climate in the Nordic seas. *Ocean Dyn.*, **65**, 223–240, doi:10.1007/s10236-014-0788-4.

Sen, P. K., 1968: Estimates of the regression coefficient based on Kendall's tau. *J. Amer. Stat. Assoc.*, **63**, 1379–1389, doi:10.1080/01621459.1968.10480934.

Sepp, M., and J. Jaagus, 2011: Changes in the activity and tracks of Arctic cyclones. *Climatic Change*, **105**, 577–595, doi:10.1007/s10584-010-9893-7.

Serreze, M. C., and R. G. Barry, 2014: *The Arctic Climate System.* 2nd ed. Cambridge Atmospheric and Space Science Series, Cambridge University Press, 395 pp.

——, and J. Stroeve, 2015: Arctic sea ice trends, variability and implications for seasonal ice forecasting. *Philos. Trans. Roy. Soc. London*, **373A**, 20140159, doi:10.1098/rsta.2014.0159.

Smith, L. C., and S. R. Stephenson, 2013: New Trans-Arctic shipping routes navigable by midcentury. *Proc. Natl. Acad. Sci. USA*, **110**, E1191–E1195, doi:10.1073/pnas.1214212110.

Squire, V. A., J. P. Duggan, P. Wadhams, P. J. Rottier, and A. J. Liu, 1995: Of ocean waves and sea ice. *Annu. Rev. Fluid Mech.*, **27**, 115–168, doi:10.1146/annurev.fl.27.010195.000555.

——, G. L. Vaughan, and L. G. Bennetts, 2009: Ocean surface wave evolvement in the Arctic Basin. *Geophys. Res. Lett.*, **36**, L22502, doi:10.1029/2009GL040676.

Stopa, J. E., and K. F. Cheung, 2014: Intercomparison of wind and wave data from the ECMWF Reanalysis Interim and the NCEP Climate Forecast System Reanalysis. *Ocean Modell.*, **75**, 65–83, doi:10.1016/j.ocemod.2013.12.006.

——, F. Ardhuin, A. Babanin, and S. Zieger, 2016a: Comparison and validation of physical wave parameterizations in spectral wave models. *Ocean Modell.*, **103**, 2–17, doi:10.1016/j.ocemod.2015.09.003.

——, ——, and F. Girard-Ardhuin, 2016b: Wave climate in the Arctic 1992–2014: Seasonality and trends. *Cryosphere*, **10**, 1605–1629, doi:10.5194/tc-10-1605-2016.

Stroeve, J. C., M. C. Serreze, M. M. Holland, J. E. Kay, J. Malanik, and A. P. Barrett, 2012: The Arctic's rapidly shrinking sea ice cover: A research synthesis. *Climatic Change*, **110**, 1005–1027, doi:10.1007/s10584-011-0101-1.

Thompson, D. W. J., and J. M. Wallace, 1998: The Arctic oscillation signature in the wintertime geopotential height and temperature fields. *Geophys. Res. Lett.*, **25**, 1297–1300, doi:10.1029/98GL00950.

Thomson, J., and W. E. Rogers, 2014: Swell and sea in the emerging Arctic Ocean. *Geophys. Res. Lett.*, **41**, 3136–3140, doi:10.1002/2014GL059983.

——, and Coauthors, 2013: Sea state and boundary layer physics of the emerging Arctic Ocean. Tech. Rep. APL-UW TR1306, Applied Physics Laboratory, University of Washington, 59 pp. [Available online at http://www.apl.washington.edu/project/project.php?id=arctic_sea_state.]

——, and Coauthors, 2016: Emerging trends in the sea state of the Beaufort and Chukchi Seas. *Ocean Modell.*, **105**, 1–12, doi:10.1016/j.ocemod.2016.02.009.

Tolman, H. L., 2003: Treatment of unresolved islands and ice in wind wave models. *Ocean Modell.*, **5**, 219–231, doi:10.1016/S1463-5003(02)00040-9.

Tran, N., F. Girard-Ardhuin, R. Ezraty, H. Feng, and P. Féménias, 2009: Defining a sea ice flag for *Envisat* altimetry mission. *IEEE Geosci. Remote Sens. Lett.*, **6**, 77–81, doi:10.1109/LGRS.2008.2005275.

Tschudi, M., C. Fowler, and J. Maslanik, 2015: EASE-Grid sea ice age, version 3. NASA National Snow and Ice Data Center, accessed 1 October 2015, doi:10.5067/1UQJWCYPVX61.

Tuomi, L., K. K. Kahma, and H. Pettersson, 2011: Wave hindcast statistics in the seasonally ice-covered Baltic Sea. *Boreal Environ. Res.*, **16**, 451–472.

Vinoth, J., and I. R. Young, 2011: Global estimates of extreme wind speed and wave height. *J. Climate*, **24**, 1647–1665, doi:10.1175/2010JCLI3680.1.

Walsh, J. E., 1991: The Arctic as a bellwether. *Nature*, **352**, 19–20, doi:10.1038/352019a0.

Wang, J., J. Zhang, E. Watanabe, M. Ikeda, K. Mizobata, J. E. Walsh, X. Bai, and B. Wu, 2009: Is the Dipole Anomaly a major driver to record lows in Arctic summer sea ice extent? *Geophys. Res. Lett.*, **36**, L05706, doi:10.1029/2008GL036706.

Wang, M., and J. E. Overland, 2012: A sea ice free summer Arctic within 30 years: An update from CMIP5 models. *Geophys. Res. Lett.*, **39**, L18501, doi:10.1029/2012GL052868.

Wang, X. L., and V. R. Swail, 2001: Changes of extreme wave heights in Northern Hemisphere oceans and related atmospheric circulation regimes. *J. Climate*, **14**, 2204–2221, doi:10.1175/1520-0442(2001)014<2204:COEWHI>2.0.CO;2.

——, Y. Feng, V. R. Swail, A. Cox, and C. Cob, 2015: Historical changes in the Beaufort–Chukchi–Bering Seas surface winds and waves, 1971–2013. *J. Climate*, **28**, 7457–7469, doi:10.1175/JCLI-D-15-0190.1.

Wilks, D. S., 2006: *Statistical Methods in the Atmospheric Sciences*. 2nd ed. International Geophysics Series, Vol. 91, Elsevier, 627 pp.

Young, I. R., 1994: Global ocean wave statistics obtained from satellite observations. *Appl. Ocean Res.*, **16**, 235–248, doi:10.1016/0141-1187(94)90023-X.

——, S. Zieger, and A. V. Babanin, 2011: Global trends in wind speed and wave height. *Science*, **332**, 451–455, doi:10.1126/science.1197219.

Zieger, S., 2010: Long-term trends in ocean wind and wave height. Ph.D. thesis, Swinburne University of Technology, 177 pp.

——, J. Vinoth, and I. R. Young, 2009: Joint calibration of multiplatform altimeter measurements of wind speed and wave height over the past 20 years. *J. Atmos. Oceanic Technol.*, **26**, 2549–2564, doi:10.1175/2009JTECHA1303.1.

——, A. V. Babanin, and A. Ribal, 2013: Wave climate in the marginal ice zone as observed by altimeters. *Fall Meeting 2013*, San Francisco, CA, Amer. Geophys. Union, Abstract OS11B-1652.

——, ——, and I. R. Young, 2014: Changes in ocean surface wind with a focus on trends in regional and monthly mean values. *Deep-Sea Res. I*, **86**, 56–67, doi:10.1016/j.dsr.2014.01.004.

——, ——, W. Erick Rogers, and I. R. Young, 2015: Observation-based source terms in the third-generation wave model WAVEWATCH. *Ocean Modell.*, **96**, 2–25, doi:10.1016/j.ocemod.2015.07.014.